Glass Laser Research

SEMIANNUAL REPORT for
Office of Naval Research
Contract No. Nonr-38 33(00)

JANUARY 1965

CORNING
CORNING GLASS WORKS

SEMIANNUAL TECHNICAL REPORT

July 1964 to December 1964

Contract Nonr - 3833(00)

January 30, 1965

Glass Laser Research

Corning Glass Works

Corning, New York

Order No. 306-62

Project Code No. 7300

Authors: CGW

R. D. Maurer

N. F. Borrelli

M. E. Vance

G. E. Stong

TRG, Inc.

S. D. Sims

J. Dennis

ABSTRACT

This report comprises a series of investigations aimed at the more efficient utilization of neodymium glass lasers. Sections 1 and 2 involve the deterioration under intense light. Damage on the cylindrical surface due to pump light has been shown due to scratches and imbedded particles. This is eliminated by chemical treatment of the surface. The mechanism of solarization is delineated and the problem eliminated by pump light filtering with a minimal 15 per cent loss in output. Sections 3 and 4 involve the improvement of performance by varying external conditions. The efficiency of various pump bands is given in detail for matching light sources. Output is further maximized by varying the cavity coupling. From these output coupling data the first "dynamic internal loss" values for a near perfect static medium are reported. They are about $0.02cm^{-1}$, three times as large as the static losses. Sections 5, 6, 7 and 8 involve processes occurring within the laser itself. A detailed investigation to find an accurate value of the gain cross section (without assuming degeneracies) shows that a straightforward spectroscopic study can only yield this quantity within a factor of two. Gain measurements in an amplifier are determined for eventual translation, through the gain cross section, into energy storage and real pump efficiency. The final section gives data on the time resolved distortion of a pumped rod to determine the magnitude of this problem in preventing diffraction limited operation. A 15cm rod, under 7000 joule electrical input to the pump light, developed a distortion of several fringes across the aperture.

TABLE OF CONTENTS

TABLE OF CONTENTS CONT'D

INTRODUCTION

Contract Nonr 3833(00) was expanded on April 30, 1964, to include more work on the utilization of glass in devices. The expanded funding was used by Corning Glass Works to subcontract TRG, Inc. for a portion of the effort. TRG, Inc. has had extensive experience in the utilization of materials in laser applications. This knowledge was deemed useful in testing glass to better define its operating parameters and using these results to suitably modify the glass properties. Within the report, Sections 3, 7 and 8 were carried out by TRG, Inc. and the others by Corning Glass Works.

Sections 1 and 2 investigate the deterioration of glass lasers under protracted use. One problem, encountered at low pumping levels, is the surface crazing from pumping light. A second problem is solarization. Solutions to both of these are described. As the light intensity is raised, damage can result from inclusions within the laser. Little data are available on this effect and the effort described here has been directed toward defining the problems -- to first measure the inclusions and later their susceptibility to damage at various power levels. Sections 3 and 4 are concerned with varying the pumping and output coupling for maximum efficiency. TRG, Inc. has knowledge of flash pump spectral efficiency versus input energy which can be used with pump band efficiency to tailor the pump light to the system. The relative efficiency of various pump bands is reported here for this purpose. There follows a section on output coupling which defines the effective dynamic internal loss.

Sections 5, 6, 7 and 8 probe further into the mechanisms within the laser itself. First there is a spectroscopic study aimed at finding an accurate value of the gain cross section per excited neodymium ion. This is necessary to translate gain into stored energy and measure absolute pumping efficiency. The stored energy can then be used with output energy to give an efficiency of extraction. Gain values have been measured and are reported. Finally, measurements of optical distortion during pumping are reported. These data point up the difficulty in obtaining diffraction limited beam spreads but glass composition variations can be used to minimize this problem.

1.0 GLASS DAMAGE UNDER INTENSE OPTICAL RADIATION (CGW)

1.1 Particulate Inclusions in Glass

Most modern optical glass is manufactured in platinum lined glass melting and fining tanks. As a result, microscopic platinum inclusions occur in optical glass, although so infrequently that they are ordinarily no problem. However, the advent of high power lasers introduced the possibility of catastrophic damage when even one such inclusion was present. Initial studies of this problem have considered the possibilities for improving the present manufacturing method, a difficult matter since it was developed at such great expense and effort. The first phase was an examination of Code 0580 laser glass to define the problem and obtain samples or data for future quantitative damage studies.

An extended study was therefore made of the incidence of particulate inclusions in Code 0580 glass. Three levels of inspection have been used - the unaided eye and a stereoscopic microscope at 7 power magnification and at 60 power magnification.

A. Unaided eye - In a total of 29 feet of 1½" diameter laser rod, 28 inclusions were observed. At least 4 of these were seeds and 1 was a stone. Most of the remaining 23 inclusions were metallic, ranging in size from perhaps 25 to 100 microns, giving about 0.04 metallic inclusions per cubic inch.

B. 7 power microscope - In seven 20" lengths of rod, 46 inclusions were observed (excluding 3 visible to the unaided eye), or about 0.2 inclusions per cubic inch. These were estimated to range in size from perhaps 5 to 25 microns. Most of these are believed to be metallic inclusions.

C. 60 power microscope - In twenty-one 1/8" thick polished slices of 1½" diameter laser rod, 26 inclusions were observed, or 5.6 inclusions per cubic inch. These ranged in size from about 1 micron to 10 microns and all were metallic.

The relative freedom from inclusions of Code 0580 glass (soda-lime silicate) may be seen by comparison with a competitive lanthanum glass #720-503, in which 315 metallic inclusions were observed with the 60 power microscope in a sample of 1.83 cubic inches, or 172 inclusions per cubic inch. These inclusions were estimated to be from 1 to 10 microns in size, with one larger inclusion of perhaps 20 microns.

Electron microprobe studies of two large metallic inclusions in Code 0580 glass indicate that one is approximately 90% lead, 10% platinum while the second is all platinum. The high lead content of the first inclusion is explained by prior lead-glass runs in the tank in which this lead-free glass was melted.

1.2 Surface Damage

Glass lasers frequently show blistered and spalled spots on the cylindrical surface after a few shots, particularly for pumping energies several times that of threshold. Such damage can be quite extensive for high input power. Spalling of from one-half to two-thirds of the cylindrical surface has been observed after two to three shots under such power.

It has been shown that such damage results from intense local heating caused by strong absorption of pumping radiation at various types of absorbers on the glass surface. These absorbers include embedded abrasive and polishing compound, checks from grinding, scratches

and general dirt. During pumping, small regions of the glass surface are heated by these absorbers to temperatures such that flow can occur and checks are then formed upon cooling at the periphery of the heated regions. Thus checks initially present will enlarge and spalling of the surface can occur over extended areas provided enough absorbing defects are present.

Surface damage can be more severe than merely blistering or spalling under very high power pumping conditions. Checks, formed in a 3 foot long laser enlarged and propagated to a depth of some 3/16" under successive pumping shots, serving within twenty shots as the source for conical fractures some 3/16" deep and 3/8" diameter. In some cases, voids of tubular shape were formed in the originating checks, where some volume of glass had vanished, either by flowing out as a liquid or by vaporization.

The flat end surfaces of lasers are not exposed to pumping radiation but the laser flux in the cavity causes pitting on these ends, from similar defects in the polished surfaces.

Complete elimination of this damage to the cylindrical surface has been achieved by removal of all of the surface defects by chemical treatment. No damage to the new surface will occur in further use provided this new surface is kept perfectly clean.

2.0 EFFECT OF SOLARIZATION ON LASER PERFORMANCE (CGW)

Solarization of glass lasers is a problem in both application and research. The solarization causes a rapid decrease in laser efficiency and output, perhaps even rendering the device inoperative, while in the laboratory this same decrease in efficiency prevents the attainment of accurate, reproducible data. A study was undertaken to find the magnitude of the solarization effect, determine its cause and prevent its occurrence. The experiment thus consisted of three phases. The first was the measurement of laser output under repeated use, the second was the measurement of associated optical absorption changes to correlate with the laser output, and the third was the use of pump light filtering to prevent the solarization.

2.1 Experimental Arrangement with Lasers

A laser rod of Code 0580 glass with polished cylindrical surface and flat ends, 6.10mm. diameter and 61mm. long, was mounted on the axis of a General Electric Xenon helical flash tube, FT-524. The laser was mounted at one end in a pin vise and was thus exposed directly to the radiation from the flash tube, with no intervening support tube. The cavity was completed by dielectric mirrors, an 85% reflecting output mirror placed about 16 inches from the laser and a 99% reflecting mirror placed about 10 inches away. The optical alignment was checked, and adjusted when necessary, prior to each shot. Input power to the flashtube was maintained at 4.6KV, giving input electrical energy of 4200 joules.

Laser output was measured using a Maser Optics Inc. calorimeter into which the output beam was directed. Under the test conditions,

output readings on the meter could be made to approximately 0.1 joule although the total precision of measurement was somewhat less.

Repetition rate varied widely since the experiment extended over several weeks. However the operation of checking and readjusting alignment imposed a minimum time of 3 minutes between shots and the time interval was frequently much longer and of the order of 30 minutes.

2.2 Laser Output in Repeated Use

A previously unused, or fresh, Code 0580 glass laser received a total of 61 shots of the flash tube, operating as a laser with output measured for 26 of these shots. Laser operation was not permitted for the majority of shots, the mirrors of the cavity being covered.

The rod was noticeably solarized after the first shot and solarization was severe after this series of shots was completed. It was therefore desolarized by heating in a furnace in air, at 375°C for 4 hours.

The desolarized laser received a total of 53 shots, again operating intermittently as a laser with output measured. The flat ends of the laser were found to be considerably pitted after the twelfth shot, the pitting being more severe on the output end. It seems probable that pitting had begun earlier but had not been observed until it had become rather severe after the twelfth shot.

Solarization was again severe after completion of the series of 53 shots and the rod was then desolarized for the second time at 375°C for 4 hours.

The laser, after the second desolarization treatment, received 16 shots from the flash tube, operating as a laser for the first seven shots and the 12th to 16th shots. The experiment was terminated after this series of 16 shots.

The results of the three series of shots are presented in Figure 2.1, where the output in joules is plotted against number of shots on a log-log chart. It is evident that straight lines give a reasonably satisfactory representation of the data for the previously unused rod, for the first eight shots of the desolarized rod and for the twice desolarized rod. Least squares lines have been calculated for these data, with these equations resulting:

1. for the previously unused rod:

$$\log \text{Output} = 0.675 - 0.202 \log (\text{Number of Shots})$$

2. for the first eight shots of the desolarized rod:

$$\log \text{Output} = 0.443 - 0.112 \log (\text{Number of Shots})$$

3. for the twice desolarized rod:

$$\log \text{Output} = 0.32 - 0.092 \log (\text{Number of Shots})$$

The rest of the data for the desolarized rod, shots 9 to 53, may possibly be explained as showing the results of pitting of the faces of the rod. Such pitting was noticed after the twelfth shot.

These data show, for these test conditions

1. Output decreases steadily with increasing number of shots;

2. After desolarization, output does not return to the original level, although some improvement is effected;

3. A second desolarization does not return the output to the level obtained after the first desolarization, but rather shows a continuing reduction in output.

2.3 Optical Absorption

The laser rod used for output power test showed sev[illegible] solarization after a number of shots, but was not a sample geometry suitable for accurate measurement of optical absorption. It was evident that a thin layer at the rod circumference had become much darker while the center of the rod had changed color. Absorption measurements made axially in the rod would not be a sensitive indicator of solarization, while measurements perpendicular to the axis would be difficult to make and interpret. A flat, thin sample in which measurements could be made through the thin surface layer appeared more suitable.

A sample of Code 0580 glass, 15 x 25mm. x 3.15mm. thick was chosen as a satisfactory test piece. This sample was supported on the axis of the FT-524 xenon flash tube using the pin vise and a sealed-on handle so that it was exposed directly to the radiation from the flash tube, with no intervening support tube. It was then subjected to the same series of 4200 joule shots as that previously given the laser rod.

Prior to any exposure to the flash tube, a spectrophotometric trace of absorption was run from 6000Å to 3000Å and in the neighborhood of 10,600Å on a Cary Model 14 Recording Spectrophotometer. The change in linear absorption coefficient $\Delta\alpha$ was computed from the increase in absorption shown on subsequent Cary traces and used as a measure of solarization.

The change in linear absorption coefficient is greatest in the ultraviolet near the UV cut-off and decreases with increasing wavelength. A small but preceptible increase thus can be observed at 6000Å. No change can be observed at 10,600Å.

The change in linear absorption coefficient of a fresh sample for three wavelengths is plotted in Figure 2.2 against number of shots on a semi-log chart. Straight lines on this semi-log charg give a reasonably satisfactory representation of the observed data. The increase in absorption evidently proceeds in the same fashion for the three wavelengths, only the rate of change being smaller as the wavelength increases.

The effect of repeated shots after desolarization (375°C for 4 hours) is shown in Figure 2.3. The same increase in absorption is seen here as in Figure 2.2. The data for 3225Å were also plotted in Figure 2.3 as the dashed line to enable direct comparison of the change in absorption before and after first desolarization. The rate of change of absorption is identical for the two cases, with absorption apparently slightly less after desolarization. A critical comparison of the initial absorption traces before and after desolarization shows that desolarization did not completely remove the absorption in the ultraviolet and the small remaining absorption from the first series of shots is enough to account for the difference shown.

The effect of repeated shots after a second desolarization of 375°C for 4 hours was the same as after the first desolarization, within experimental error.

The change in linear absorption coefficient is seen to be an essentially completely reversible effect for the desolarization schedule used. However, the laser output is not restored to its original value by the same desolarization schedule. The drop in output of the laser as solarization proceeds cannot then be due solely to increased absorption of the pump light by the stronger coloration of the glass.

2.4 Fluorescence of Solarized 0580 Glass

It is the purpose here to measure the fluorescence intensity of samples of 0580 glass, in solarized, desolarized and unsolarized conditions, to ascertain whether there is any correlation with the laser output measurements reported above.

Slabs of glass 15 x 25 x 3mm. were prepared in three conditions; 1) unsolarized, 2) solarized after 20 shots of 4200 joules and 3) desolarized after solarization of 10 shots. The fluorescence spectra, of these three samples, (whose absorption spectra are shown in Fig. 2.4) were measured in the same manner as described before in Fig. 5.2 except the monochromator slits were opened to essentially collect the fluorescence over the full 1.06μ line. Corning filters were used to isolate particular regions of the excitation spectra to see if the effectiveness of these portions were changing with the solarization condition. Table 2.4 presents the data where the results are expressed as the ratio of the fluorescence intensity with a specified filter to that with no filter.

Table 2.4

Corning Filter	Transmission Region	Desolarized	Unsolarized	Solarized
3850	> 3500Å	0.95 ± 10%	0.96 ± 10%	0.96 ± 10%
3384	> 4950Å	0.79 "	0.81 "	0.81 "
3482	> 5400Å	0.91 "	0.91 "	0.91 "
2030	> 6600Å	0.74 "	0.77 "	0.78 "
9788	3300 >λ<7000Å	0.12 "	0.11 "	0.10 "
Rel. Intensity no filter		161 ± 6%	168 ± 6%	171 ± 6%

The results indicate that there is no significant change within the accuracy of the measurement, of the relative contribution of the various pumping regions to the fluorescent intensity. It should be noted that there appears to be an inversion of order between the 3384 and the 3482 filter. This is due to the absorption of the 3384 filter in the near infrared, about 30%, which overlaps the near infrared pump band thus reducing the intensity. This points out that the data in Table 4.4 should only be compared for the same filter since the results have not been corrected for the transmission of the filters.

These results leave unclear the role of solarization in laser performance. It has been shown that optical absorption of pump light cannot explain the deterioration nor is there a decrease in fluorescence efficiency. Data from TRG on fluorescence efficiency (reported below) indicate a small decrease but no change in fluorescence large enough to account for the observed laser output changes. The exact cause of the deterioration from pump light is still under investigation.

2.5 Elimination of Solarization by Selective Filtering of Pump Light

Since solarization of the laser glass results in a reduction of the laser output, it seems worthwhile to look at the effect of filters inserted between the pump light and the laser rod. In this way, the solarization producing portion of the pump light might be filtered out at the minimum expense to the laser energy output. Tubes of filter glasses having the absorption spectrum shown in Fig. 2.5A were slipped over the laser rod. The threshold and laser energy output at an input of 4200 joules, were measured for the two filters as well as for no

filter. These results are shown in Fig. 2.5B.

A rough estimate of the contribution of portions of the excitation spectrum to the laser output can be made as follows. The output energy can be written as

$$E_{out} = K \langle\alpha\rangle (E_{in} - E_o) \frac{\beta}{\beta+1}$$

where

K is a constant which includes efficiency of electrical energy to light, and geometry

$\langle\alpha\rangle$ is effective absorption coefficient

E_{in} is input energy

E_o is threshold power

β is coupling coefficient = $\frac{1/t_{coup}}{1/t_{int.\ loss}}$

The results are listed below.

Region	$K\langle\alpha\rangle/(K\langle\alpha\rangle)_o$
$\lambda \gtrsim 6000$Å	0.45
$4750 \leq \lambda \leq 6000$	0.40
$\lambda \lesssim 4750$	0.15

It is seen that the output dropped and the threshold increased corresponding to the degree of filtering of the pump light. In order to determine whether Fresnel reflection losses from the tube contributed to the output drop a VYCOR® brand tube of the same diameter was placed over the rod. The energy output and threshold for this arrangement as compared to the no filter and the 3555 filter is shown in Fig. 2.6A. This indicates that no such reflection losses occur.

Fig. 2.6B show the measured output for the 3555 filter arrangement as a function of number of 4200j shots compared to that in a

no-filter arrangement. It is seen that the output for the filtered rod remains essentially unchanged over fifty shots. This filtering provides a partial solution to the solarization problem with minimal loss in efficiency.

3.0 SPECTRAL PUMPING EFFICIENCY (TRG, INC)

3.1 Statement of the Problem

Spectral transmission data for laser glass is generally useful in locating and measuring widths of pump bands. However, much meaningful information essential to engineering of laser devices cannot be derived by this method, namely the effectiveness or efficiency of each of the absorption bands. Pumping efficiency information leads to the selection of pumping sources best suited for the laser glass and permits possible filtering of the pump light to reject light in absorption bands which contribute little to the laser output. Such filtering may preclude unnecessary thermal distortion of the laser rods and corresponding output losses due to absorption of pump light which does not efficiently contribute to the output. Rejection of light in the short wavelength absorption regions, which may degrade performance due to solarization, may also be accomplished.

3.2 Description of the Experiments

A photofluorometer was designed and fabricated. This device permits a sample of laser material to be irradiated by a light source and measures the resultant fluorescence. Two methods of operation are possible with the photofluorometer. The first method utilizes a series of filters to irradiate the sample in six selected bands between 35 and 900 nanometers:

a.) broadband - between 400 and 900 nanometers

b.) 360 nanometers

c.) 500 to 650 nanometers

d.) 750 nanometers

d.) 800 and 880 nanometers

e.) 880 nanometers.

This method is considered to be particularly adapted to comparative source evaluation for a given glass sample. In the second method the sample is irradiated with monochromatic light as from a monochrometer which may be scanned over the spectrum with high resolution. The pumping efficiency is obtained. This method was used to obtain the results reported and is considered suitable for evaluation of various glass compositions.

Figure 3.1 is a block diagram of the experiment. The pumping light source was an Osram XBO 150 xenon high pressure compact arc lamp operated by 60 cycle per second a.c. This lamp provided a modulated source of high brightness with a broad and fairly continuous spectrum. The light was focussed on the entrance aperture of a Perkin-Elmer grating monochromator. An order sorting filter of Schott BG18 or RG-8 filter glass was installed at the entrance aperture. The monochrometer band width was 2 nanometers and the spectrum was scanned in steps of approximately 3 nanometers.

The monochromator exit slit is imaged on an Eppley thermopile which monitors the output energy. A beam splitter diverts approximately half of the output energy to an image coinciding with the external image of the photo fluorometer field stop. The image of the monochromator exit slit is therefore the pump source of the photofluorometer. Fluorescence is detected as 120 cycle signal corresponding to the modulation of the xenon arc lamp.

The photofluorometer consists of a lens system which focusses the pumping source with unit magnification on a field stop 1mm x 10mm. Immediately behind the field stop is the laser glass sample, a tile 12mm x 12mm x 2mm. One large face of the tile is aluminized. Fluorescence emerging through the other large face is collected by a lens system into the phototube (RCA 7102) through an Optics Technology Inc. 1.068μ interference filter and a Corning 57-56 filter.

The data recorded are wavelength, relative fluorescence intensity (phototube signal), and pump light intensity. A correction is made for spectral transimission of the beam splitter. Relative pumping efficiency is defined as the ratio of phototube signal to thermopile signal.

The sample whose relative spectral pumping efficiency was measured was Corning laser glass Code 0580. Code 0580 glass exhibits solarization which causes a decrease of laser output accompanied by a color change in the glass. A solarization coefficient has been defined as the change in the absorption coefficient per centimeter from its initial value. Two tiles, 12mm x 12mm x 1.8mm were cut from the same large cane of glass. One of the tiles was exposed to approximately 5000 flashes at about one inch from a lamp in a circular polished enclosure. The lamp was an E G & G FX 38 operated at 200 joules. The transmission of the unexposed and exposed specimen were 0.90 and 0.74 at 400 nanometers respectively yielding an absorption coefficient due to solarization of 1.09 per centimeter.

3.3 Results

Results are presented in Fig. 3.2. Relative pumping efficiency is plotted against wavelength between 300 and 900 nanometers. Measurements were made on two specimens, one which was not exposed to laser pump light shown by the solid curve, another which had an absorption coefficient due to solarization of 1.09 per centimeter shown by the dashed curve.

Relative pumping efficiency is derived from the ratio of fluorescence intensity to pump light intensity. A correction for spectral variation in the beam splitter has been made.

3.4 Analysis

It can be seen in Fig. 3.2 that efficient pumping does not necessarily coincide with the strongest absorption bands. Fluorescence was not detected for irradiation in the strong 355 nanometer absorption band. Conversely the relatively weak absorption at 530 nanometers yields efficient fluorescence.

The effect of solarization on the pumping efficiency is easily seen. The efficiency of the solarized tile as shown by the dashed curve drops severely in the 530, 573 and 586 nanometer bands, and slightly in the 430 and 475 nanometer bands. No effect was noted in the red and infrared bands for this degree of solarization. A graphic integration of these curves yields a 12 percent drop in efficiency for pump light of uniform spectral radiance.

The transmission spectra of these tiles is in Fig. 3.3. The solarized tile shows a decrease in transmission over the entire spectrum which is most severe at shorter wavelengths. With the exception of the

band 355 nanometers, the absorption bands do not appear to be affected. It seems unlikely therefore that the drop of laser output for solarized glass or the preferential drop in spectral efficiency can be explained in terms of additive absorption.

The spectral transmission of a solarized sample was almost entirely restored as a result of several hours bakeout at 350°C.

3.5 Future Plans

Three experiments are planned in connection with this study.

a.) Degree of restoration of spectral pumping efficiency possible in the solarized specimen by baking the specimen.

b.) Effect of spectral pump filtering on efficiency and solarization.

c.) Measurement of relative spectral pumping efficiency of other samples that Corning may provide.

4.0 TOTAL ENERGY OUTPUT (CGW)

The total energy output of a Code 0580 glass laser has been measured for various levels of excitation and output coupling and for various amounts of mirror misalignment. This was performed with a TRG Model 106 Laser Power Source, Pulse Forming Network and Flash Head. This system employs two EG + G FX-47A flashtubes in a double elliptical pumping enclosure mounted between external mirrors.

4.1 Optical Alignment

The mirrors M_1 and M_2, indicated in Figure 1, were first made parallel by means of an autocollimator located to the left of M_1. Then the flash head, containing the laser rod, was inserted between the mirrors, and the left face of the laser - visible through the partly transparent mirror M_1 - was made parallel to M_1. Since the laser faces are non-parallel by 4 seconds or arc, a light beam perpendicular to M_1 would be deviated by about 2 seconds for a laser of refractive index 1.5, as illustrated in Figure 4.1. The system is thus effectively misaligned by about 2 seconds of arc, but reproducibly so.

Throughout the experiments to be described the mirror separation was 85cm. The output energy passed through M_2 and was focussed into a TRG Model 101 Ballistic Thermopile the output of which was measured with a Kiethley 150A Microvolt-ammeter. The laser was a 12.5cm long by 1cm diameter rod of Code 0580 laser glass with an unpolished cylindrical surface. It was surrounded by a yellow glass (Corning Code 3555) tube to remove ultraviolet pumping light and prevent solarization. This laser rod had been previously subjected to 625 pump pulses of near-threshold intensity and was visibly solarized.

The output energy was found to be strongly dependent on mirror misalignment. Figure 4.2 shows relative energy output versus the angular displacement θ of mirror M_1 from correct alignment as described above. Curve A is for conditions of low output coupling and low excitation. The reflectance R_1 of M_1 was 99% and the reflectance R_2 of M_2 was 95%. The input energy relative to input energy at threshold $\frac{E_{in}}{E_T}$ in this case was 1.04. Curve B shows the behavior for the same output coupling at the higher excitation level $E_{in}/E_T = 2.9$. Curve C was obtained for high output coupling (R_1 = 99%, R_2 = 30%) and a moderate excitation level $E_{in}/E_T = 2.1$.

The laser rod itself could be tilted out of alignment by 30 seconds of arc without affecting the energy output by more than 10 per cent.

4.2 Output Versus Input for Various Values of Output Coupling

The total energy output as a function of input electrical energy to the flashtubes for various output mirror reflectances R_2 is plotted in Figures 4.3 and 4.4. The values for $E_{in} \leq 2000j$ were obtained with capacitances of 750 and 1500 microfarads. Each experimental point represents the average of several determinations. The standard deviation was about 5% except near threshold, where it was as high as 50%.

In all cases R_1 was 0.982 and R_2 took the values shown. Reflectances were determined by independent reflectance and transmittance measurements on the mirrors, which had multilayer dielectric reflecting films on one side and antireflection coatings on the other. For example, the result for the 95% mirror was R = 0.953, transmittance T = 0.042, R + T = 0.995, leaving 0.005 for absorption by the films, a not unreasonable value.

The laser ends were uncoated and no allowance has been made for the effect of Fresnel reflection at the laser-air interface.

4.3 Calculation of Dynamic Loss Coefficient

For a constant pump pulse shape the input energy threshold E_T should be proportional to the total laser cavity loss[1], which may be expressed as the sum of a dynamic internal loss coefficient α_i and an effective output loss coefficient $\frac{-\ln R_1 R_2}{2\ell}$ where ℓ is the length of the laser rod. That is

$$E_T = K(-\ln R_1 R_2 + 2\ell\alpha_i)$$

If E_T is plotted against $-\ln R_1 R_2$ the value of α_i can be obtained from the slope and intercept of the resulting straight line. If E_{To}, the threshold for no output coupling, is this intercept, α_i can be calculated from

$$\alpha_i = \frac{E_{To}}{2\ell K}$$

The lowest threshold, 337j, was obtained with two 99.0 per cent reflecting mirrors, while the others correspond to the E_{in} - intercepts of Figure 4.4. These experimentally determined thresholds are plotted versus $-\ln R_1 R_2$ in Figure 4.5. A best-fit straight line is extrapolated to the E_T axis. The result of the calculation for this laser is $\alpha_i = 0.024 \pm .005\text{cm}^{-1}$. The Fresnel reflection at the laser rod faces should increase the effective value of $R_1 R_2$. A calculation of this effect shows that α_i may have as low a value as 0.016cm^{-1} for this laser. This idea is being pursued by repeating the measurements with antireflection coatings on the rod faces.

The result has been obtained on a laser of almost perfect optical quality and for which the static losses are extremely well known.[2]

These static losses are $0.006cm^{-1}$, or about one third to one fourth the value of the dynamic loss.

4.4 Optimum Output Coupling

The data of Figures 4.3 and 4.4 are replotted in Figure 4.6 to give curves of E_{out} versus $R_1 R_2$ for various pumping energies designated by the parameter E_{in}/E_{To}, where E_{To} = 315j is the threshold input energy for zero output coupling obtained from Figure 4.5. Each curve of Figure 4.6 reaches a maximum at a different value of $R_1 R_2$. These optimum values of $R_1 R_2$ are plotted against E_{in}/E_{To} in Figure 4.7; for a given pump energy there exists an optimum output coupling for maximum energy output.

5.0 SPECTROSCOPY OF NEODYMIUM IN GLASS: GAIN CROSS SECTION (CGW)

The gain cross section at 1.06μ per excited neodymium ion is useful to know in many studies of glass lasers. For instance, it is necessary in order to convert gain measurements into stored energy. Attempts have been made to obtain a value for this quantity but all of them require some assumptions about the degeneracy of states. A more detailed study to obtain the degeneracies, or g-values, is reported below; it utilizes the thermal variation of optical absorption and fluorescence. However, the results cannot be adequately described by the free ion degeneracies and some more accurate theoretical approach appears necessary to get a reliable value for the gain cross section by the homogeneous line assumption.

5.1 Theory

The laser material under study here is a soda lime glass doped with trivalent Neodymium. The energy level schemes for a Nd free ion and an ion in the soda lime environment are reproduced in Figure 5.1. The lowest lying free ion states are the $^4F_{3/2}$ and the ^4I multiplets which are (2J+1) fold degenerate. In a glass it may be assumed that the Nd ion enters the network in a modifying position; for each particular set of neighbors the Nd ion energy levels are slightly different so that the observed energy level scheme in glass may be considered to be an average over all possible configurations. The resulting splittings are not generated by a unique process and so a theoretical assignment of degeneracies can not be made. However, it is tentatively assumed that the sum of the level degeneracies within a given state is equal to the free ion value.

When the laser is pumped, electrons from the ground state are lifted into energy states corresponding to the strong absorption bands. These electrons lose energy and cascade to the $^4F_{3/2}$ levels. These levels are metastable since transitions to the lower lying ^4I states are forbidden by simple selection rules.

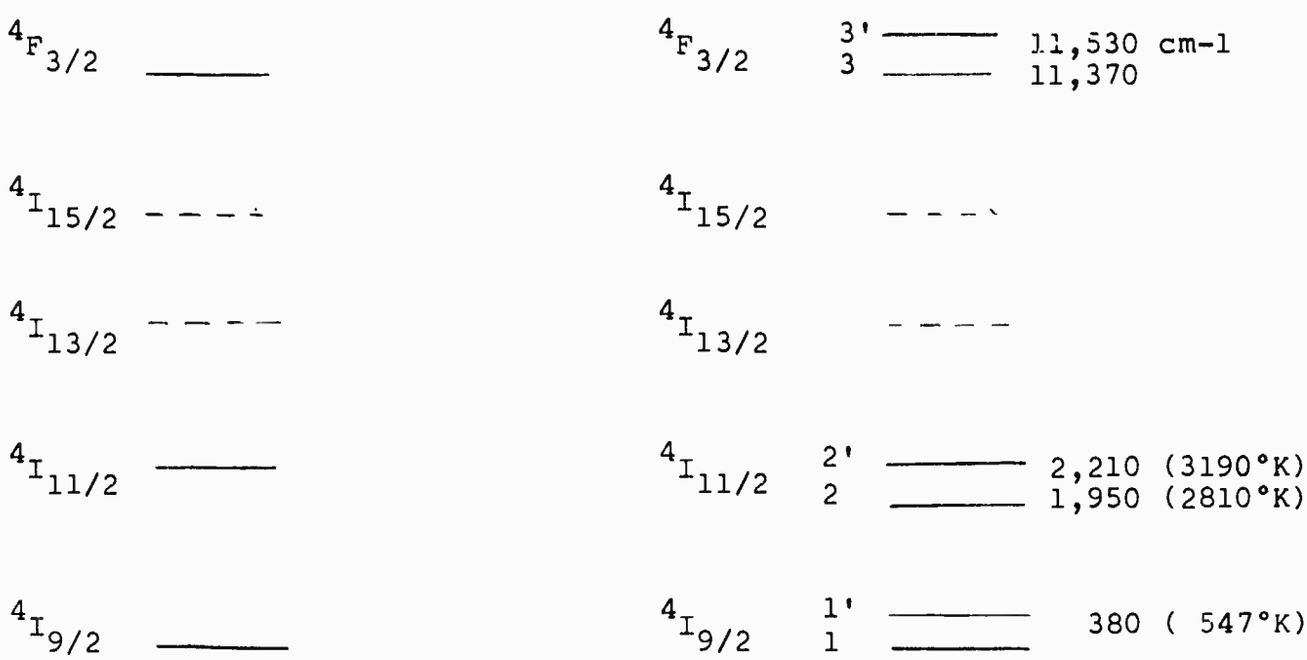

Figure 5.1 (a) Free ion energy level scheme. (b) Nd^{3+} energy level scheme in soda lime glass.

Of particular interest here is the transition from the lower $^4F_{3/2}$ level to the lower $^4I_{11/2}$ level accompanied by the emission of radiation bout 1.06μ.

The first method by which a value of the 1.06μ induced emission rate can be calculated will now be considered. Electrons in the $F_{3/2}$ levels decay to all of the I levels, emitting characteristic radiation called fluorescence. The fluorescence consists of many lines grouped

in four sets about 0.89μ, 1.06μ, 1.35μ, and 1.82μ, at frequencies corresponding to the energy level differences. Each transition has its own spontaneous rate and the sum of these rates is equal to the total emission rate from the $F_{3/2}$ state, the reciprocal of the measured fluorescence lifetime. It is assumed that the areas under the fluorescence line at a given frequency is proportional to the probability that an electron decays from the $F_{3/2}$ fluorescence lifetime, the spontaneous emission rate for any of these lines can be calculated. In particular, the rate for the 1.061 transition is obtained in this way, from which a value of the corresponding induced rate is calculated using the first Einstein relation. (i.e. the relation between A & B).

This method appears to be straightforward; however, several complications arise in carrying it through. First, within a given state the splittings induced by the glass environment are small and, in addition, the line widths of the fluorescence lines are broad. Therefore, the fluorescence from the $F_{3/2}$ state to an I state consists of a cluster of lines which are hard to resolve. To determine the area under a given line requires some guesswork in the form of curve fitting. Second, the value of the $F_{3/2}$ lifetime is not clearly defined. The lifetime is measured by pumping the glass with a short pulse of light and observing the decay of the 1.06μ fluorescence as a function of time. A semilog plot of the intensity as a function of time should be a straight line whose slope gives a value of the lifetime. When this is done for a Nd glass, a straight line does not result; the "lifetime" increases with elapsed time. This effect can be explained by assuming that different Nd sites in the glass have different transitions rates so that the observed

decay is a weighted sum of exponentials with different lifetimes.[4] In this work an average value of the lifetime was taken and, as a result, the rate calculated from it represents an average value for the system. Third, in addition to decaying with the emission of fluorescence, a certain number of electrons in the upper level are lost by a process called quenching. (See Section 2) The total transition rate from the $F_{3/2}$ state is then a sum over the quenching rate and the spontaneous emission rates for all of the transitions to the I states.

$$A_{F_{3/2}} = \Sigma_i \, A^i_{F \rightarrow I} + A_q \qquad 5.1$$

$$A_q = p \, N_o^2 \qquad 5.2$$

The second method by which a value of the 1.06μ induced emission rate can be calculated will now be considered. By measuring the absorption rate about 1.061μ, the induced emission rate for this transition can be calculated using the second Einstein relation, (i.e. the relation between B's), if the level degeneracies were known. The integrated absorption for this line is related to the absorption rate by the expression:

$$\int k(\nu) d\nu = K \frac{\pi}{2} k_m \Delta\nu = \frac{h\nu_o \eta}{c} B_{23} \, n_2 \qquad 5.3$$

where $k(\nu)$ is the absorption coefficient at a particular frequency and n_2 is the population of the lower $I_{11/2}$ level. At room temperature this population is negligible since the effective temperature of this level is 2810°K. However, by heating the glass this level is thermally populated and absorption is observed. The distribution of Nd ions among the various energy levels in thermal equilibrium is governed by Boltzmann statistics:

$$\frac{n_1}{g_1} = \frac{n'}{g'_1} \exp(-547/T) = \frac{n_2}{g_2} \exp(-2810/T) = \frac{n'_2}{g'_2} \rho(-3180/T) \qquad 5.4$$

$$n_1 + n'_1 + n_2 + n'_2 + \ldots\ldots\ldots\ldots\ldots = N_o \qquad 5.5$$

where the energy of the level has been expressed as an effective temperature, T is the temperature of the glass in degrees Kelvin, and N_o is the concentration of Nd ions. Once again the level degeneracies (g) are not known.

To overcome the dilemma presented by these unknown degeneracies, the following procedure will be adopted. Values are assigned to the degeneracies assuming that their sum within a given state is equal to the free ion value. The induced emission rate, calculated in this way, is compared to the value obtained by the fluorescence study to check the assignment. Fluorescence and absorption curves are also measured for the 0.89μline and the same procedure can be used as a further check. In addition, comparing the ground state absorption at room temperature to that at an elevated temperature is an excellent method of determining the ground state degeneracies since the adjustment of the population at higher temperatures decreases the absorption from the lower level and increases the absorption from the upper levels. It is worth emphasizing that the absorption rates, determined in this way, represent an average over the distribution of values at different sites in the medium. Analogous to the fluorescence curves, the absorption curve consists of a number of closely spaced lines. To separate one transition requires fitting a few Lorentzian lineshapes to the experimental data, each with its own height, central frequency, and linewidth.

5.2 Experimental Details

5.2.1 Fluorescence

A sketch of the apparatus for measuring fluorescence curves is given in Figure 5.2. Light from a tungsten lamp is chopped, focussed, led through a defining aperture, and passed through the glass

sample. Part of the fluorescence radiation is collected by the slit and lens system and focussed on the entrance slit of the Leiss monochromator. The fused silica prism in the monochromator selects a band of wavelengths about a central wavelength, determined by the drum setting, and passes it through the exit slit onto the detector. The resolution of the monochromator is set by the openings of the entrance and exit slits and the dispersion of the prism. The signal generated by the detector is picked up by the lock-in amplifier which amplifies only the signal in phase with the reference located behind the chopper. The amplified signal is displayed as a "Y" deflection on the recorder as a function of the "X" sweep which is driven in synchronism with the drum. Two detectors are used: a Kodak Type N1 lead sulfide (PbS) photodiode for wavelengths greater than 1μ and a selected RCA 7102 photomultiplier, cooled with dry ice and acetone, for wavelengths less than 1.15μ.

The curves obtained in this way are a graph of recorder deflection as a function of drum setting. The drum readings are converted to wavelength units by calibrating the monochromator with the lines of mercury discharge. The recorder deflection is corrected for spectral response of the apparatus as a function of wavelength by calibrating the response with a black body source.

5.2.2 Absorption

The apparatus for measuring the absorption of the Nd glass is illustrated in Figure 5.3. Light from a tungsten source is collected by the leading mirrors and focussed to a converging beam in the region C-D, then collected by the back mirrors and focussed on the entrance slit of the Perkin-Elmer monochromator. The signal from the

detector is amplified and displayed on a recorder as a function of the drum setting. A fused silica prism was used with a slit opening of 50μ giving a resolution of 16Å. The wavelength calibration for the drum was made using the lines of a mercury discharge.

The Nd glass samples, 1½" x 5/16" x 5/16", were placed in a holder equipped with circular apertures on each end to define the path of the light through the sample. Thermocouples are attached to the middle of the sample and at one end with Sauereisen to insure good thermal contact. The samples were inserted in a furnace, equipped with fused silica windows to reduce thermal gradients across the samples. In addition, the furnace, 7" long with a diameter of 1 1/8", was constructed with additional windings on the ends to reduce gradients. At 500°C, the gradient across the sample was less than 2°C.

Two samples were placed in the furnace side by side at the same time: one is the Nd glass with an index of refraction of 1.533 whose absorption is to be measured and the other is a glass with a closely matching index of 1.517 which acts as a reference. By sliding the furnace, it is possible to pass the light beam through either the Nd glass sample of the reference. Over the wavelength interval for which the absorption is measured, the transmission of the reference and of the sample is taken as a function of drum reading. Since the two glasses are similar, except for the Nd absorption, a ratio of these transmittances, normalized to 1.0 away from absorption regions, gives the transmission losses due to the Nd absorption. This transmission loss can be converted to absorption and expressed as an absorption oefficient by dividing by the length of the samples.

5.3 Data

The fluorescence curves about 0.88μ, 1.06μ, and 1.35μ were determined in the manner described above and are shown in figures 5.4, 5.5 and 5.6. In addition the fluorescence about 1.82μ was observed using a powerful xenon arc source and decreased resolution and this curve, referred to the same intensity standard, is shown in figure 5.7. It is interesting to note that the fluorescence about 1.35μ and 1.82μ overlap in the wavelength region near 1.6μ. From these curves it can readily be seen that the fluorescence about any central wavelength consists of a number of incompletely resolved peaks: four in the case of 0.88μ and 1.06μ and an undetermined number in the case of 1.35μ and 1.82μ.

A set of fluorescence curves were measured for two glasses: glass A with 0.89×10^{20} Nd ions/cc and glass B with 4.4×10^{20} Nd ions/cc. The areas under the fluorescence curves, proportional to the probability that an electron makes a given transition , are tabulated below for these two glasses.

Wavelengths Range	Area Ratio A	B
0.88μ	0.925	0.877
1.06μ	1.000	1.000
1.35μ	0.140	0.166
1.82μ	0.0072	

The lower ratio for the 0.88μ fluorescence of glass B is readily explained as self absorption which is certainly stronger for a glass with increased Nd concentration. The higher ratio for the 1.35μ fluorescence of glass B results from a better determination of this curve over that for glass A

using a quieter recorder. In spite of these rationalizations, these ratios are substantially the same; from this it is inferred that the atomic transition rates are not dependent on the Nd ion concentration in the Nd glass laser system. In other words, the radiative fluorescence lifetime is a constant and the observed variation of the lifetime with Nd ion concentration is due entirely to the quenching mechanism whose rate is assumed to depend on the square of the concentration.

The exact magnitude of this fluorescence lifetime is open to question. A semilog plot of fluorescence intensity as a function of time does not give a straight line and there is no unique lifetime.[2] In this work average lifetime values were used; however, the validity of this interpretation will be examined later. The mean lifetime of glass A (0.89×10^{20} 1/cc) is 525 μsec. and of glass B (4.4×10^{20} 1/cc) is 340 μsec; from these numbers the average fluorescence transition rate and the quenching rate can be calculated.

$$\frac{1}{t} = A_F + A_q$$

$$A_q = P\, N_o^2$$

$$A_F = 1.866 \times 10^3 \text{sec}^{-1}$$

$$P = 0.055 \times 10^3 \text{sec}^{-1}\ [10^{-40}\ \text{cm}^6]$$

From these numbers the variation of the observed lifetime as a function of the Nd ion concentration can be evaluated

$$T = \frac{1000\ \mu\text{sec}}{1.866 + 0.055\ [N_o \times 10^{-20}]^2} \qquad 5.6$$

This function is plotted in Figure 5.8 as a solid line; experimental

points are indicated on this plot as open circles. The exceptional agreement substantiates the assumptions that the radiative probability is independent of the Nd ion concentration and that the quenching rate depends on the square of this concentration. This functional form indicates that the quenching rate is probably due to the resonance transfer mechanism discussed below; however, the final test of this model rests on its ability to predict the correct magnitude for the parameter P from the overlap integral of the combined fluorescence about 1.35μ and 1.82μ and the absorption about 1.6μ. This integral is evaluated and will be discussed later.

In figures 5.9 and 5.10, the absorption about 0.88μ for glass A is shown for two temperatures: 25°C. and 522°C. The appearance of new peaks and the depression of existing ones at the higher temperatures illustrates the thermal adjustment of the ground level populations. In figure 5.11 the absorption from the terminal laser level to the upper level is shown for glass B at 510°C. In this case thermal population of the intermediate level results in a noticeable absorption, which is absent at room temperature. Finally, in figure 5.12 the resonance absroption about 1.6μ is displayed for glass B at room temperature.

5.4 Calculations

The first item to be calculated are the degeneracies of the ground state levels from the absorption about 0.88μ at room temperature and at 522°C. To this end the four lines making up the 0.88μ curve are defined in Fig. 5.1, viz transitions $1 \rightarrow 3$, $1 \rightarrow 3'$, $1' \rightarrow 3$ and $1' \rightarrow 3'$.

At room temperature, the intermediate levels are negligibly populated so that

$$n_1 + n_1' = N_o$$

$$n_1' = \frac{g_1'}{g_1} \; n_1 \; e^{-547°K/298°K}$$

$$= n_1 \; \frac{g_1'}{g_1} \; (0.158)$$

So the populations of the gound state at T = 25°C are expressed in terms of the degeneracies as

$$n_1 = N_o \; [1 + \frac{g_1'}{g_1} \; 0.159]^{-1}$$

$$n_1' = N_o \; [\frac{g_1'}{g_1} \; 0.159] \; [1 + \frac{g_1'}{g_1}]^{-1}$$

At the elevated temperature, 522°C, the population of the intermediate level must be reckoned, as it results in a depopulation of the ground state.

$$n_1 + n_1' + n_2 + n_2' = N_o$$

$$n_1' = \frac{g_1'}{g_1} \; n_1 \; e^{-547/795} = \frac{g_1'}{g_1} \; n_1 \quad (0.503)$$

$$n_2 = \frac{g_2}{g_1} \; n_1 \; e^{-2810/795} = \frac{g_2}{g_1} \; n_1 \quad (0.0292)$$

$$n_2' = \frac{g_2'}{g_1} \; n_1 \; e^{-3190/795} \; \frac{g_2'}{g_1} \; n_1 \quad (0.0189)$$

Combining these results, the populations of the ground state levels at 522°C. are (the values used for $g_2 + g_2'$ are relatively unimportant. Here $g_2 = g_2'$ is taken to be 6.)

$$n_1 = N_o \left[1 + \frac{g_1'}{g_1} (0.503) + \frac{6}{g_1} (0.0481)\right]^{-1}$$

$$n_1' = N_o \frac{g_1'}{g_1} (0.503) \left[1 + \frac{g_1'}{g_1} (0.503) + \frac{6}{g_1} (0.0481)\right]^{-1}$$

In the table below, the relative values of the populations are given for the two temperatures as a function of the degeneracy assignments.

Table 5.1

g_1	g_1'	$\frac{n_1 (25°C)}{n_1 (522°C)}$	$\frac{n_1 (25°C)}{n_1 (522°C)}$
8	2	1.12	0.352
6	4	1.25	0.395
4	6	1.47	0.465
2	8	1.92	0.610

This table is significant since the population is determined experimentally from the two absorption curves. At a given temperature the integrated absorption coefficient is related to the population by:

$$K = \pi \, km \, \left(\frac{\Delta\nu}{2}\right) = \frac{h\nu_o \eta}{c} B_{13} \, n_1 \qquad 5.7$$

For a given line the only quantities which vary with temperature are the population, the peak absorption coefficient, and the half width. Therefore the ratios are experimentally determined as follows:

$$\frac{n_1 (25°C)}{n_1 (522°C)} = \frac{(km \, \Delta\nu) (25°C)}{(km \, \Delta\nu) (522°C)} \qquad 5.8$$

with a similar relationship for n_1'. By fitting four Lorentzian curves

to the absorption data, the individual lines can be isolated. When this is done for these two curves, the following fits are obtained:

Table 5.2

T = 25°C	$-\Delta\nu/2 = 2.75$	10^{12}cps.
$k_1 = 1.25 \times 10^{-1}$ cm^{-1}		$\nu_1 = 3.415$ 10^{14}cps.
$k_2 = 3.60 \times 10^{-1}$ cm^{-1}		$\nu_2 = 3.365$ 10^{14}cps.
$k_3 = 0.375 \times 10^{-1}$ cm^{-1}		$\nu_3 = 3.305$ 10^{14}cps.
$k_4 = 0.22 \times 10^{-1}$ cm^{-1}		$\nu_4 = 3.255$ 10^{14}cps.
T = 522°C	$\Delta\nu/2 = 3.31$	10^{12}cps.
$k_1 = 0.78 \times 10^{-1}$ cm^{-1}		$\nu_1 = 3.410$ 10^{14}cps.
$k_2 = 2.25 \times 10^{-1}$ cm^{-1}		$\nu_2 = 3.360$ 10^{14}cps.
$k_3 = 0.74 \times 10^{-1}$ cm^{-1}		$\nu_3 = 3.300$ 10^{14}cps.
$k_4 = 0.44 \times 10^{-1}$ cm^{-1}		$\nu_4 = 3.250$ 10^{14}cps.

From these fits the following ratios are obtained:

$$\frac{n_1\ (25°C)}{n_1\ (522°C)} = 1.33 \qquad \frac{n_1'\ (25°C)}{n_1'\ (522°C)} = 0.421 \qquad 5.9$$

This means that the only possibilities for the ground state degeneracies are either $g_1 = 6$, $g_1' = 4$ or $g_1 = 4$, $g_1' = 6$, if their sum is to equal the free ion value of 10. The inability to distinguish more closely is due to the slight freedom allowed by the fits and the intrinsic experimental uncertainty.

With this result as a guide, the magnitudes of the stimulated emission rates from the upper levels to the ground state levels will now be calculated from the room temperature absorption data.

$$n_1 = 0.89 \times 10^{20} \text{ 1/cc } [1 + \frac{g_1'}{g_1} 0.159]^{-1}$$

$$n_1' = 0.159 \times \frac{g_1'}{g_1} \times 0.89 \times 10^{20} \text{ 1/cc } [1 + \frac{g_1'}{g_1} 0.159]^{-1} \qquad 5.10$$

$$B_{13} = \frac{\pi k(m)(\frac{\Delta\nu}{2})}{h(\frac{\nu_o}{c})\,\eta\, n_1}$$

The following quantities are substituted:

$k(m)$ = units of 10^{-1} cm^{-1}

$\frac{\Delta\nu}{2}$ = units $2.75\ 10^{12}$ cps.

$h = 6.624 \times 10^{-34}$ joule-sec

$\frac{\nu_o}{c} = \frac{1}{\lambda}$ units of 10^4 cm^{-1}

$\eta = 1.533$

After these substitutions are made and using the second Einstein relation

$$g_1 B_{13} = g_3 B_{31} \qquad 5.11$$

and the specific numbers obtained from the fits to the data, Table 5.2, the rates are in units of 10^{21} 1/sec/joule-sec/cc.

$$\begin{matrix} B_{3'1} \\ B_{31} \\ B_{3'1'} \\ B_{31'} \end{matrix} = \begin{matrix} 1.02\ g_1/g_{3'} \\ 3.02\ g_1/g_3 \\ 2.02\ g_1/g_{3'} \\ 1.20\ g_1/g_3 \end{matrix} [1 + \frac{g_1'}{g_1} 0.159] \qquad 5.12$$

Now these rates will be calculated from the fluorescence about 0.88μ. Here again the curve is synthesized by fitting four Loretzian lineshapes of a given height and half width to the data. In arbitrary units the best fit is:

$f_1 = 1.30$ $\lambda_1 = 0.885\mu$

$f_2 = 3.85$ $\lambda_2 = 0.8975\mu$

$f_3 = 2.40$ $\lambda_3 = 0.9125\mu$

$f_4 = 1.40$ $\lambda_4 = 0.9275\mu$

8.95

The total fluorescence transition rate is $1.866\ 10^3$ 1/sec. and the average values of the integrated fluorescence areas are tabulated below:

Table 5.3

Intensity		Quanta
A(.88μ)	= 0.9000	0.7470
A(1.06μ)	= 1.0600	1.0000
A(1.35μ)	= .1530	.1950
A(1.82μ)	= .0072	.0124

Combining these results the spontaneous transition rates for the transitions making up the 0.88μ fluorescence can be calculated.

$$A = \frac{.747}{1.954} \quad \frac{f}{8.95} \quad 1.866\ \ 10^3 \text{ 1/sec} \qquad 5.13$$

The corresponding stimulated rates can be calculated from the first Einstein relation.

$$A = \frac{8\ \pi\ h\ \ \nu_o^3\ \ \eta^3}{c^3} \quad B \qquad 5.14$$

$$B = \frac{1.32\ f\ x\ 10^{21}\ \text{1/sec}}{\left(\frac{1}{\lambda}\right)^3\ \ \frac{\text{joule-sec}}{\text{cc}}}$$

Combining these results the following rates are reported, where for convenience the stimulated rate is expressed in units of 10^{21} 1/sec/joule-sec/cc.

Table 5.4

(1) $\lambda_1 = 0.868\mu$

$A_{3'1} = 102$ 1/sec

$A_{3'1} = 1.12$

(2) $\lambda_2 = 0.880\mu$

$A_{31} = 306$ 1/sec

$B_{31} = 3.48$

(3) $\lambda_3 = 0.897\mu$

$A_{3'1'} = 191$ 1/sec

$B_{3'1'} = 2.28$

(4) $\lambda_4 = 0.910\mu$

$A_{31}' = 111$ 1/sec

$B_{31}' = 1.39$

Comparing these stimulated rates to the corresponding ones calculated from absorption it is readily seen that:

$$\frac{g_1}{g_{3'}}\left[1 + \frac{g_1'}{g_1}\,0.159\right] = \begin{matrix}1.10\\1.13\end{matrix} \qquad \frac{g_1}{g_3}\left[1 + \frac{g_1'}{g_1}\,0.159\right] = \begin{matrix}1.15\\1.16\end{matrix} \quad 5.15$$

The interpretation of these results will be discussed later.

Now the absorption about 1.06μ at 510°C. is considered. The lines making up the 1.06μ absorption are defined in Fig. 5.1 viz transitions $2 \rightarrow 3$, $2 \rightarrow 3'$, $2' \rightarrow 3$ and $2' \rightarrow 3'$.

The populations are given by the following expression which is valid to about 3%.

$$n_2 = \frac{g_2}{g_1}\, n_1 e^{-2810/783} = \frac{g_2}{g_1}\,(0.0276)\, N_o\,(1+\frac{g_1'}{g_1}\,0.498)^{-1}$$

$$n_2' = \frac{g_2'}{g_1}\, n_1 e^{-3.190/783} = \frac{g_2'}{g_2}\,(0.0171)\, N_o\,(1+\frac{g_1'}{g_1}\,0.498)^{-1} \quad 5.16$$

where $N_o = 4.4 \times 10^{20}$ 1/cc. Fitting lineshapes to the data, the following quantities are obtained:

Table 5.5

$T = 510°C \quad (\frac{\Delta\nu}{2}) = 3.31 \times 10^{12}$ cps.

(1) $k_1 = 0.90 \quad (\frac{1}{\lambda})_1 = 0.958$

(2) $k_2 = 5.80 \quad (\frac{1}{\lambda})_2 = 0.942$

(3) $k_3 = 2.40 \quad (\frac{1}{\lambda})_3 = 0.932$

(4) $k_4 = 1.15 \quad (\frac{1}{\lambda})_4 = 0.916$

The stimulated rates in units of 10^{21} 1/sec/joule-sec/cc. are:

$$\begin{matrix} B_{3'2} \\ B_{32} \\ B_{3'2} \\ B_{32'} \end{matrix} = \begin{matrix} 0.805 \; g_1/g_3' \\ 5.25 \; g_1/g_3 \\ 3.50 \; g_1/g_3' \\ 1.71 \; g_1/g_3 \end{matrix} \left[1 + \frac{g_1'}{g_1} \; 0.498\right] \qquad 5.17$$

These same rates will be calculated below from the fluorescence about 1.06μ. In arbitrary units the best fits are:

Table 5.6

$f_1 = 0.70$	$\lambda_1 = 1.044$
$f_2 = 4.45$	$\lambda_2 = 1.061$
$f_3 = 2.90$	$\lambda_3 = 1.072$
$f_4 = 1.35$	$\lambda_4 = 1.092$

The spontaneous transition rates are:

$$A = \frac{1.0}{1.9544} \quad \frac{f}{9.40} \quad 1.866 \; 10^3 \text{ 1/sec} \qquad 5.18$$

$$= 101.4 \; f \; \text{sec}^{-1}$$

and the stimulated rates are given by:

$$B = 0.160 \times 10^{21} \frac{f}{(\frac{1}{\lambda})^3} \quad . \quad \text{1/sec/joule-sec/cc} \qquad 5.19$$

Substituting the fits the following rates are reported, where the stimulated rates are expressed in units of 10^{21} 1/sec/joule-sec/cc.

Table 5.7

(1) $\lambda_1 = 1.044\mu$	(2) $\lambda_2 = 1.061\mu$
$A_{3'2} = 71$ 1/sec	$A_{32} = 452$ 1/sec
$B_{3'2} = 1.29$	$B_{32} = 8.43$
(3) $\lambda_3 = 1.072\mu$	(4) $\lambda_4 = 1.092\mu$
$A_{3'2} = 294$ 1/sec	$A_{32'} = 137$ 1/sec
$B_{3'2'} = 5.62$	$B_{32'} = 2.71$

Once again a comparison of these rates to those calculated from absorption gives for each line, a value of the undetermined quantity arising from the multiplicities. These values are:

$$\frac{g_1}{g_3'}\left[1 + \frac{g_1'}{g_1}\, 0.498\right] = \begin{matrix} 1.60 \\ 1.60 \end{matrix} \qquad \frac{g_1}{g_3}\left[1 + \frac{g_1'}{g_1}\, 0.498\right] = \begin{matrix} 1.60 \\ 1.59 \end{matrix} \qquad 5.20$$

It is perhaps best here to digress from the calculations to explain the procedure used to obtain these fits. Each curve is made up by the contributions of four unresolved lines. The frequencies of these lines have been determined from low temperature data by Maurer.[4] In this work the lines were not seen at the same positions; however, this is probably due to a calibration error. The frequency (or wavelength) for one line can be picked out because there is always one prominent

line and the other frequencies are assigned by uniformly displacing the set of frequencies. For all lines the same halfwidth is taken, usually determined by trial and error. The heights are the only parameters left and these are varied to obtain the best fit. In addition some limited freedom is taken with the position of the central frequency of the lines. This freedom might destroy confidence in the results obtained from these fits; the fits made in this way to both the absorption data and the fluorescence data must give values for the stimulated rates which are consistent, such as the agreement illustrated immediately above. This tends to renew confidence in the method.

Returning to the calculation, the important rates to which this work is directed are the rates for the 1.061μ line. First, its spontaneous rate is 452 1/sec compared to a total fluorescence rate from the $F_{3/2}$ level of 1,866 1/sec. If all of the electrons which are pumped into the absorption band drop to the $F_{3/2}$ levels, then the ratio of these rates is the quantum efficiency. At any rate an upper bound on this parameter is q = 0.242.

5.5 Discussion

For the strongest frequency in the 0.88μ group, the stimulated emission rates are

$$B_{31} = 3.48 \quad 10^{21} \qquad \text{(fluorescence)}$$

$$B_{31} = 3.02 \times 10^{21} \quad \frac{g_1}{g_3}\left(1 + \frac{g_1'}{g_1}\, 0.159\right) \qquad \text{(absorption)}$$

and for the 1.061μ line the stimulated rates are:

$$B_{32} = 8.43 \quad 10^{21} \qquad \text{(fluorescence)}$$

$$B_{32} = 5.25 \quad 10^{21} \quad \frac{g_1}{g_3}\left(1 + \frac{g_1'}{g_1}\, 0.498\right) \qquad \text{(absorption)}$$

The following set of degeneracies are assumed $g_1 = 4$ $g_1' = 6$ $g_3 = 2$. These are consistent with the assumption that the sum of the level degeneracies for a given state must equal the free ion value, consistent with the 0.88μ absorption data presented earlier, and they give the lowest rates consistent with these requirements.

$B_{31} = 7.47 \quad 10^{21}$ (absorption)

$B_{32} = 18.35 \quad 10^{21}$ (absorption)

<u>These rates are about twice as large as the corresponding rates obtained from fluorescence</u>. The purpose of the following discussion is to consider the reason for this discrepancy.

First, if the fluorescence value is assumed to be reliable then the following quantities result

$$\frac{g_1}{g_3} \left(1 + \frac{g_1'}{g_1} 0.159\right) = 1.16$$

$$\frac{g_1}{g_3} \left(1 + \frac{g_1'}{g_1} 0.498\right) = 1.60$$

Using $g_1 = g_3 = g_3'$ and $g_1' = \frac{3}{2} g_1$, these ratios are 1.24 and 1.75 respectively. Such an assignment could arise in the following way. For the gound state $g_1 = 4$, $g_1' = 6$ which gives $g_3 = g_3' = 4$. The $F_{3/2}$ state should have $g_3 = g_3' = 2$; the additional degeneracy could arise from low lying $F_{5/2}$ levels. This is possible since the F multiplets are closely spaced, as evidenced from the absorption spectra. The rates which result from this assignment are:

$B_{31} = 3.48 \times 10^{21}$ (fluorescence)

3.74×10^{21} (absorption)

$B_{32} = 8.43 \times 10^{21}$ (fluorescence)

9.15×10^{21} (absorption)

This suggests that the area under the 1.06μ fluorescence is too low or that the 1.06μ absorption is too strong. The difference between these two rates sets the experimental uncertainty at about ± 4%. Using the average rate, the 1.06μ gain cross section is:

$$\sigma_m (1.061) = (0.97^5 \pm 0.04) \times 10^{-20} \text{ cm}^2$$

An alternative explanation is that some of the transitions from the crystal field split ground state to the $^4F_{3/2}$ states are forbidden and hence $g_1 + g_1' \neq 10$. However to carry through the calculation of the distribution of populations within these states one would need to know the energy of the forbidden levels. The selection rules governing forced dipole transitions are extremely difficult to obtain since the transitions are allowed through mixing of the f^3 configuration with those of opposite parity e.g. $4f^2$ 5d. Without explicit knowledge of the wavefunctions of these mixed configurations and the symmetry of the crystal field operator[6] one cannot simply determine whether all of the $^4I - {}^4F$ transitions involved are allowed or not.

Thus it appears that in order to bring together the stimulated emission coefficients computed from emission data and from the absorption measurement one must have a detailed description of the energy levels of Nd^{3+} in a glass matrix.

6.0 SPECTROSCOPY OF NEODYMIUM IN GLASS: QUENCHING PROBABILITY (CGW)

A resonance transfer mechanism has been proposed by Dexter and Schulman[5] to explain this process. The essential features of this mechanism are the following. Certain electrons in the $F_{3/2}$ state make transitions to the $I_{15/2}$ and $I_{13/2}$ states with the emission of fluorescence radiation of the proper frequency to be absorbed by an electron in the ground state raising it to the $I_{15/2}$ state. Once in this resonance state, the energy is rapidly lost and, as a result, the $F_{3/2}$ state has been depopulated without the observation of an emission photon. The quenching rate A_q is given by the expression:

$$A_q = \frac{9}{16\ \pi^2} \qquad \frac{\beta^2}{R^6} \qquad A'_r \qquad 6.1$$

$$\beta = [\frac{4\pi\hbar^4 c^4}{3\eta^4} \qquad A \int f_a\ (e)\ f_e\ (e)\ \frac{dE}{E^4}]^{\frac{1}{2}} \qquad 6.2$$

where A'_r is the transition rate for the fluorescence line, A is an oscillator strength for the absorption from the ground state to the $I_{15/2}$ level, $f_a(e)$ and $f_e(e)$ are normalized lineshapes for the absorption and emission curves, and R is the mean distance between Nd ions. The important parameter is the overlap integral and equally significant is the fact that the quenching rate is proportional to the square of the Nd ion concentration. Data will be presented to support this explanation.

From Eqn. 6.1 with the assumption[5] that $1/N = \frac{4\pi}{3} R^3$ avg, the quenching probability is given by

$$A_q = A'_r\ \beta^2\ N^2 \qquad 6.3$$

where these terms are defined as before. The radiative probability is readily obtained from the ratio of the area under the emission curve

given in Fig. 5.7 to the total area under all of the fluorescence lines, multiplied by the total radiative probability. This yields a value of $A_r' = 0.053 \times 10^3$ sec^{-1}. From the absorption and emission data of Figs. 5.7 and 5.12 the value of β was computed by machine computation. The resulting value of β was, $\beta = 0.278 \times 10^{20}$ cm^3. The product $A_r' \beta^2$ is computed as 0.0045×10^{-37} cm^6/sec. This number is then compared to the value obtained from the experimental variation of lifetime with concentration assuming an N^2 dependence of the quenching probability. This number, given before, is 0.055×10^{-37} cm^6/sec. It seems then that, although the resonance quenching mechanism leading to the N^2 dependence of the quenching probability fits the experimental data quite well, the overlap of the emission and absorption curves in the region 1.4 -- 2.3μ is not sufficient to account for the magnitude of the effect.

7.0 GAIN MEASUREMENTS (TRG, INC)

7.1 Statement of the Problem

The dynamic performance of laser oscillators and amplifiers can be predicted from a knowledge of the gain coefficient of the laser rod. In addition, the gain coefficient is linearly related to the stored energy so that a knowledge of the gain is sufficient to characterize the maximum available laser outputs in both Q-switched and normal modes. For this reason a series of experiments are being performed to determine the gain of a particular laser system employing a Corning Code 0580 glass laser rod. Measurements of gain versus time and pumping energy will be obtained.

7.2 Description of the Experiment

The experiment consists of making time resolved gain measurements on glass laser rods during the pumping cycle. Using an auxiliary Q-switched laser oscillator as a probe synchronized to pumping cycle of an amplifier, direct recordings of the input - output amplifier signals are obtained. Amplifier gain is measured as a function of time and input energy.

The amplifier is a nominal 7.2cm long Corning Code 0580 glass rod which is pumped in a focussed cavity of circular cross section. The pumping source is an E G & G FX42A.

Fig. 7.1 is a functional block diagram of the experiment. The probe oscillator is a glass laser which is Q-switched by a spinning prism. The pumping enclosure of the oscillator is identical to that of the amplifier. A magnetic pickup on the Q-switch prism mounting provides an electrical pulse 355 microseconds prior to alignment of the prism.

This signal is used to trigger the flashlamp of the oscillator, and the amplifier after an appropriate delay.

The beam entering and leaving the amplifier is sampled by a beamsplitter.

The energies are measured by phototubes, which are irradiated by the reflection from black diffuse targets. The phototubes are RCA Type 7102 whose output signals are integrated to provide a measure of the energies. The inputs to the phototubes are filtered by Optics Technology interference filters which pass 1.06 microns and several Schott neutral filters having a transmission of the order of 10^{-8} at 1.06 microns.

It has been found convenient to consider the timing of the experiment in two sections, early and late probing of the amplifier (Fig. 7.2). Early probing corresponds to triggering the oscillator before the amplifier so that the probe signal occurs at the beginning of the pumping pulse of the amplifier. Maximum probing time occurs when both pumping pulses begin simultaneously, in which case the amplifier can be probed only 355 microseconds after the beginning of the pumping pulse. Late probing corresponds to triggering the oscillator after the triggering of the amplifier. Late probing is accomplished by delaying the pumping of the oscillator by an integral number of magnetic pickup pulse periods.

The integrated phototube signals are recorded and measured using a dual beam oscilloscope.

7.3 Analysis

It is convenient to express the amplifier gain in terms of the gain per unit length of the material. The gain coefficient is related

to the measured overall gain by the following expression:

$$G = G_o e^{\alpha \ell}$$

where

G = ratio of output to input signal = measured overall gain

G_o = ratio of output to input signal when the amplifier is not pumped

α = gain coefficient in cm^{-1}

ℓ = length of rod in cm

Since the gain is measured in terms of the ratio of output to input signals, the method is insensitive to fluctuations of the oscillator output.

A gain of 1 or gain coefficient of 0 is defined as the ratio of output to input when the amplifier is not pumped. The gain measured is therefore the internal gain, since the conditions for the definition of gain coefficient = 0 as used here includes the reflective losses of the amplifier.

The amplifier is supported at each end by snug fitting collars which cover 5.2mm on each end of the amplifier. The portion of the rod obscured from direct pump light in a 7.2cm rod is 13 percent of the lengtn. Some excitation will occur in this region since the irradiated cylinder of the rod has a diffuse surface. An analysis of the effective flux in this portion of the rod has not been made. However, it is estimated that this will contribute less than 10 percent to the value of the gain coefficient computed.

In addition, it is necessary to keep the probe pulse energy well below the saturation level. This level can be expressed in terms of

$$\frac{E_s}{A} = \frac{h\nu}{\sigma}$$

where

E_s = integrated pulse energy

A = amplifier cross section

ν = laser frequency

λ = Plank's constant

σ = interaction cross section at the laser wavelength

E_s is the input energy which will reduce the energy stored in a differential amplifier slab to $\frac{1}{e}$ of the original value. The exact cross section for the transition is not precisely known, but is of order $1 \times 10^{-20} cm^2$.

$$\frac{E_s}{A} \approx 19 \text{ joules/cm}^2$$

Since a 1cm amplifier aperture was used in these experiments, the resulting E_s is

$$E_s \approx 15 \text{ joules}$$

The maximum amplifier output energy obtained in the experiments was 0.5 joules, which is well below the saturation level.

Finally, it should be mentioned that no attempt was made to spatially resolve the gain across the amplifier aperture. Thus the results represent the amplifier gain averaged over the amplifier aperture.

7.4 Results

Fig. 7.3 is the pump light intensity waveform in the amplifier. The maximum intensity is achieved in approximately 200 microseconds, the duration at one half peak intensity in approximately 350 microseconds. The gain vs. time results reported are contingent upon this pumping pulse. A different pumping waveform would be expected to yield a different shape

of the gain vs. time curve.

Fig. 7.4 is a curve of gain coefficient vs. time for early probing of the amplifier.

It is also observed that the curve ascends regularly to 355 microseconds which is the last data point for early probing. We expect the curve to level off and descend beyond this point as pumping ceases.

In the assembly and checkout of the apparatus it was observed that the gain measured was dependent upon the duty cycle. The measurements reported were made with regular two minute intervals between points. The dependence of gain on duty cycle under fixed probing conditions will be investigated.

7.5 Plans for the Next Period

During the next period we expect to complete data collection for the 7.2cm rods and determine the following results:

a) Gain coefficient vs. time for various input energies.

b) Gain coefficient vs. duty cycle at a fixed time and input energy.

c) Gain vs. x and y positions to be made at a fixed time measured across the output face of the amplifier.

8.0 DYNAMIC OPTICAL PATH DISTORTIONS IN A Nd-GLASS LASER ROD (TRG,INC)

8.1 Statement of the Problem

One of the important parameters of laser performance is the amplitude and phase distribution over the beam aperture. This distribution is sufficient to specify the output angular radiance (or angular energy distribution) of the laser. The distribution in turn, is dependent upon the optical quality of the glass. Mode selection as a means of increasing the spectral radiance will only work for good quality glass. For a better understanding of laser performance, one needs to know how the glass distorts a plane wave.

Great efforts have been made to obtain high optical quality Nd-glass-rods. However, the "high-quality" refers to an unpumped Nd-glass rod. What one really wants to know is the optical distortions of the glass while undergoing pumping.

The major contribution to any change of the glass optical properties will come from the heating of the rod by the pump lamps.

Optical distortion can be conveniently observed interferometrically. In particular, a Mach-Zehnder interferometer can be used to measure the change in optical path length across the aperture. Since the degree of distortion is a function of time during the pumping pulse, it is necessary to obtain time resolved interferograms through the use of either a high speed framing camera or a pulsed light source. In the particular experiments described here, a Q-switched ruby laser was used as the light source.

8.2 Description of the Experiments

A very useful tool for measurement of small changes in refractive indices for samples of large sizes is the March-Zehnder interferometer (M-Z). This instrument is schematically illustrated in Fig. 8.1. The light source is a TRG Vireo-single-lamp ruby laser. It provides a single, linearly polarized, 300m joule pulse of 30n sec duration. We will call this light pulse the "probe light." The probe light is reflected off a Schott UG-8 glass plate close to Brewster's angle in order to achieve appropriate attenuation. It then passes through a telescope of magnification M = 4 and enters the M-Z, where it is split into two parts of equal intensity at the semi-reflecting surface A_1. The two beams are then reflected from the mirrors M_1, M_2, and recombined at the semi-reflecting surface A_2. The beam splitters, D_1, D_2 are adjusted so that the second surfaces B_1 and B_2 are at Brewster's angle for the probe light, thus eliminating second surface reflection. If all reflecting surfaces are exactly parallel, a plane wave going through the M-Z would give fringes to infinity.

In general however the wavefronts of the two beams are mutually inclined and the light forms straight fringes parallel to their intersection. By adjusting M_1, M_2, D_1 or D_2 one can change the fringe-density. It is these wedge fringes that are used in the examination of our Nd-glass sample.

A glass laser sample rod (Corning Code 0580 Nd-glass-rod of 15cm length and 1.5cm diameter) was placed in one arm of the M-Z. This crystal was mounted in a TRG-XP1 laser head, consisting of two EGG-FX 47A flash lamps and a focusing reflector of double cylindrical geometry.

The flashlamps were fed by a PFN which delivered 7000 joules into the lamps during a 2.3m sec long pulse.

As was described in Section (8.1) the optical pathlength of the sample will undergo changes during and after the flashlamp pulse due to heating of the sample. This results in a change of the interferogram obtained with the M-Z and subsequently photographed.

The beam divergence of the TRG-VIREO laser output is 3×10^{-3} rad, which means that the area of coherence in a beam cross-section is 0.2mm in diameter. Therefore, one can allow 0.2mm shear of the two beam parts without extinguishing the fringe visibility. The telescope (Fig. 8.1) increased the coherence length (across the aperture) by a factor of 4, and thus improved the fringe visibility. Since a certain amount of shearing is unavoidable in practice, the telescope appeared to be necessary for obtaining good fringe visibility. Unfortunately the telescope introduced a small alteration of the plane wavefront resulting in slightly S-shaped fringes (Fig. 8.2). The telescope has the additional advantage of beam expansion, thus allowing complete filling of the aperture of the glass rod.

Although the use of a Q-switched laser as probe light source introduced the described instrumental complication in order to achieve satisfactory fringe visibility, it appeared to be the only convenient light source of desirable monochromaticity together with sufficient energy during the short 30n sec - exposure time. (2m joule/cm^2 leaving the telescope.) The 30n sec exposure time provides an extremely high time resolution for the investigation of optical path length changes in the sample as a function of time.

Besides having a refractive index greater than 1, the Nd-glass sample exhibits absorption for the probe light. Since good fringe visibility (contrast) depends not only on high coherence and small shear, but also upon the fact that the two interfering beams have equal intensity, one has to insert an attenuator in one arm of the M-Z in order to match the attenuation of the sample.

Interferograms were made at different times before, during and after the pump-pulse. Figure 8.2 shows the arrangements which were made to produce proper timing of the sample pump pulse and the probe pulse. A magnetic head pulse is available from the probe laser a fixed time before the prism reaches its alignment position. This signal appears 1100 μsec before lineup No. 1 and triggers the two delay units. One delay unit delivers a signal 3600 μsec later (T = 3600 μsec is the period of the rotating prism). This signal triggers the flashlamp of the TRG vireo. At time, t = 4700 μsec, line up No. 2 occurs and this time the probe pulse will be generated.

The second, variable delay unit delivers (in the example of Fig. 8.2) a signal at time t = 3000 μsec, which triggers the FX 47A lamps, which pump and heat the sample. The FX 47A's pulse is finished at time t = 5300 μsec, hence, the probe light occurs 1700 μsec after the FX 47A's pump pulse.

Fig. 8.3 shows a series of interferograms taken at various times before, during and after the pulse. The slightly S-shaped fringes make gradual changes in time. On one side a structure of closed lines emerges.

8.3 Results and Analysis

The eight interferograms in Fig. 8.3 show the development of a whirlpool fringe structure with the center on the right side. A fringe represents a constant phase of the light wave. Neighboring fringes correspond to a 2π phase-difference or a path difference of one wavelength. The change of intensity of the center of the whirlpool indicates movement of the center.

The results have not yet been carefully evaluated, and Fig. 8.3 is only the beginning of our extended series of interferograms which will be taken. The proposed method of evaluation of these photographs is to make contour maps of the optical path length[7]. The fringes are the geometrical loci of constant optical path length. If one can follow the movement of individual fringes in time one could tell for every point on the sample face, the time dependent optical path length change. We are planning to do this by making the time differences between interferograms short enough so that the motion of individual fringes can be followed. This should enable us to observe the absolute optical path length change. This requires sufficient repeatibility of the interferograms, which was indeed observed. The interferograms in Fig. 10 show only the relative change in optical path length for different points on the sample aperture.

In order to obtain some preliminary information, the mapping of Fig. 8.3 has been done according to Ref. 7. A linear cut was taken through the fringe pattern following the direction of maximum distortion. Fig. 8.4 shows the result.

The curves show

a) the phase ϕ vs x corresponding to Fig. 8.3e

b) the phase ϕ vs x corresponding to Fig. 8.3b

c) the difference of curves a and b

Curve c illustrates the effect of the heated crystal on a plane wave. Curve b results from the intersection of two essentially plane waves which are mutually inclined. Subtraction of a and b unravels the distortion of one wavefront caused by the heated rod. Alternatively, it represents the variation in optical path length across the rod aperture, in one plane.

The optical path length change $\delta p = nd\ell + \ell dn$ is a function of the refractive index change dn and the physical sample length change $d\ell$. We have not yet made an effort to separate both contributions. The ultimate aim of these experiments is to gather information about the optical distortions during a laser pulse caused by heating of the active crystal, and the effect of these optical distortions on the laser performance. Therefore one is most interested in total optical path length change, rather than in the contribution from the two parameters: refraction index n and crystal length ℓ.

It should be mentioned that the Nd glass was not lasing; it was merely pumped. Furthermore, since the probe light was of wavelength $\lambda_R = 6943\text{Å}$, which is far removed from the Nd laser wavelength, $\lambda_{Nd} = 1.06\mu$, the pumping and resulting population inversion had no effect on the refractive index.

The whirlpool is not symmetrically located in the sample. Preliminary measurements seem to indicate that one side of the double

cylindrical reflecting pump-enc.osure has lower reflectivity than the other.

Further detailed measurements have to be done to unravel the peculiar structure of the whirlpool.

3.4 Plans

Since the interferograms taken so far exhibit good fringe visibility and repeatibility, we have confidence that we can succeed in measuring the absolute change of the optical path length at any point of the sample face. A detailed mapping of the contour lines of constant optical path length and its change in time will be performed. The fringe structure shall be investigated for its dependence on the pumping arrangement and pump power.

In order to determine whether the fringe changes represent increases or decreases in the optical path length, a fringe counting experiment will be performed.

REFERENCES

1. T. C. MacAvoy, et. al.
Annual Technical Report for ONR Contract Nonr-3833(00) June, 1963

2. T. C. MacAvoy, et. al.
Annual Technical Report for ONR Contract Nonr-3833(00) January, 1964

3. P. Mauer, Appl. Opt. 3, 433 (1964)

4. R. D. Maurer, Proceedings of the Symposium on Optical Masers, Polytechnic Institute of Brooklyn, 1963, pp. 435-47.

5. D. L. Dexter & J. H. Schulman, Journal of Chemical Physics, 22 1063, (1964)

6. B. R. Judd, Phys. Rev. 127, 750 (1962)

7. G. W. Dueker, C. M. Kellington, M. Katzmann and J. G. Atwood, Appl. Opt. 4, 109 (1965)

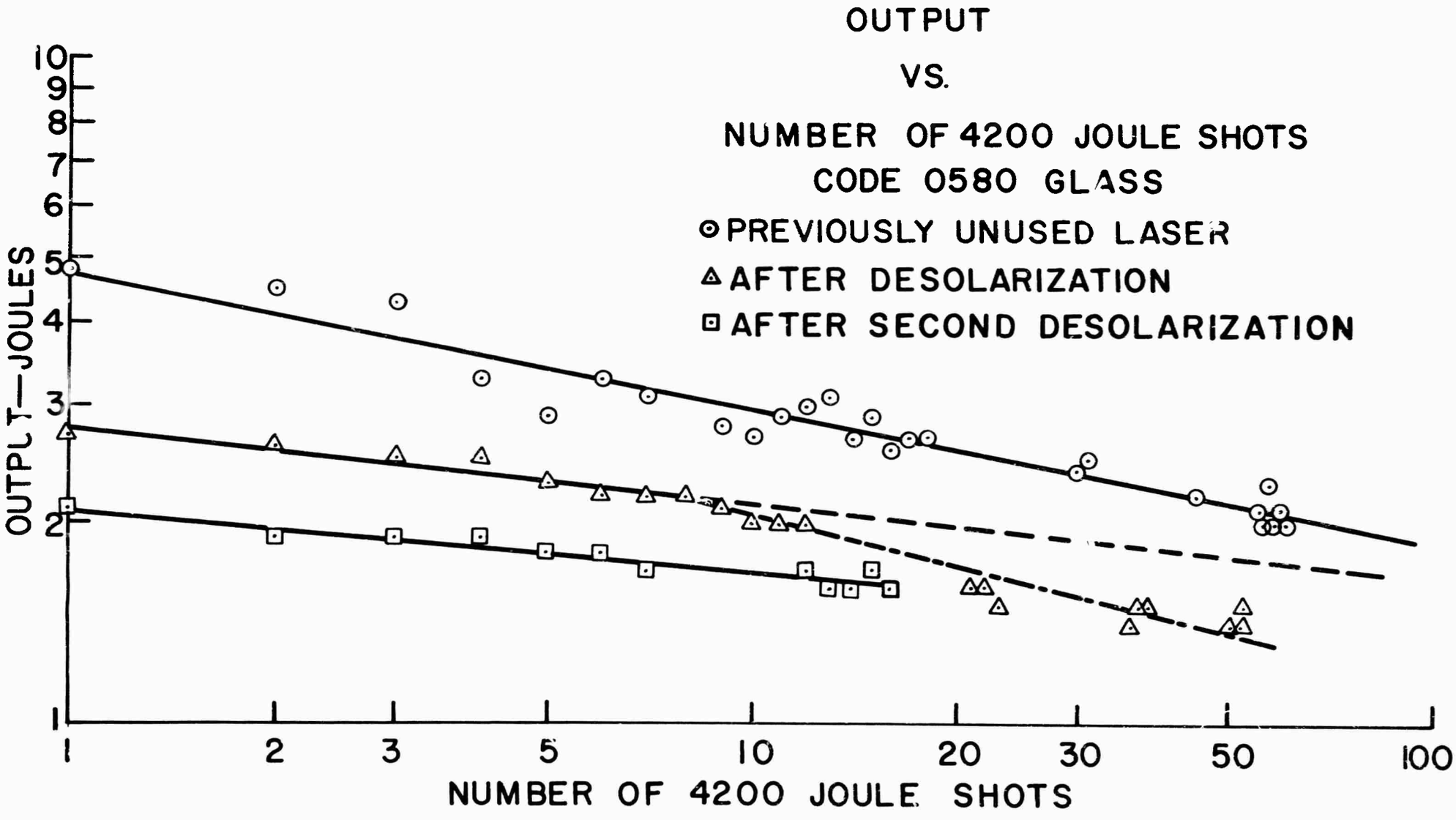
OUTPUT
VS.
NUMBER OF 4200 JOULE SHOTS
CODE 0580 GLASS
PREVIOUSLY UNUSED LASER
AFTER DESOLARIZATION
AFTER SECOND DESOLARIZATION
OUTPUT—JOULES
10
9
8
7
6
5
4
3
2
1
1
2
3
5
10
20
30
50
100
NUMBER OF 4200 JOULE SHOTS

Fig. 2.1

Increase of Optical Absorption in a Fresh Laser Due to Solarization

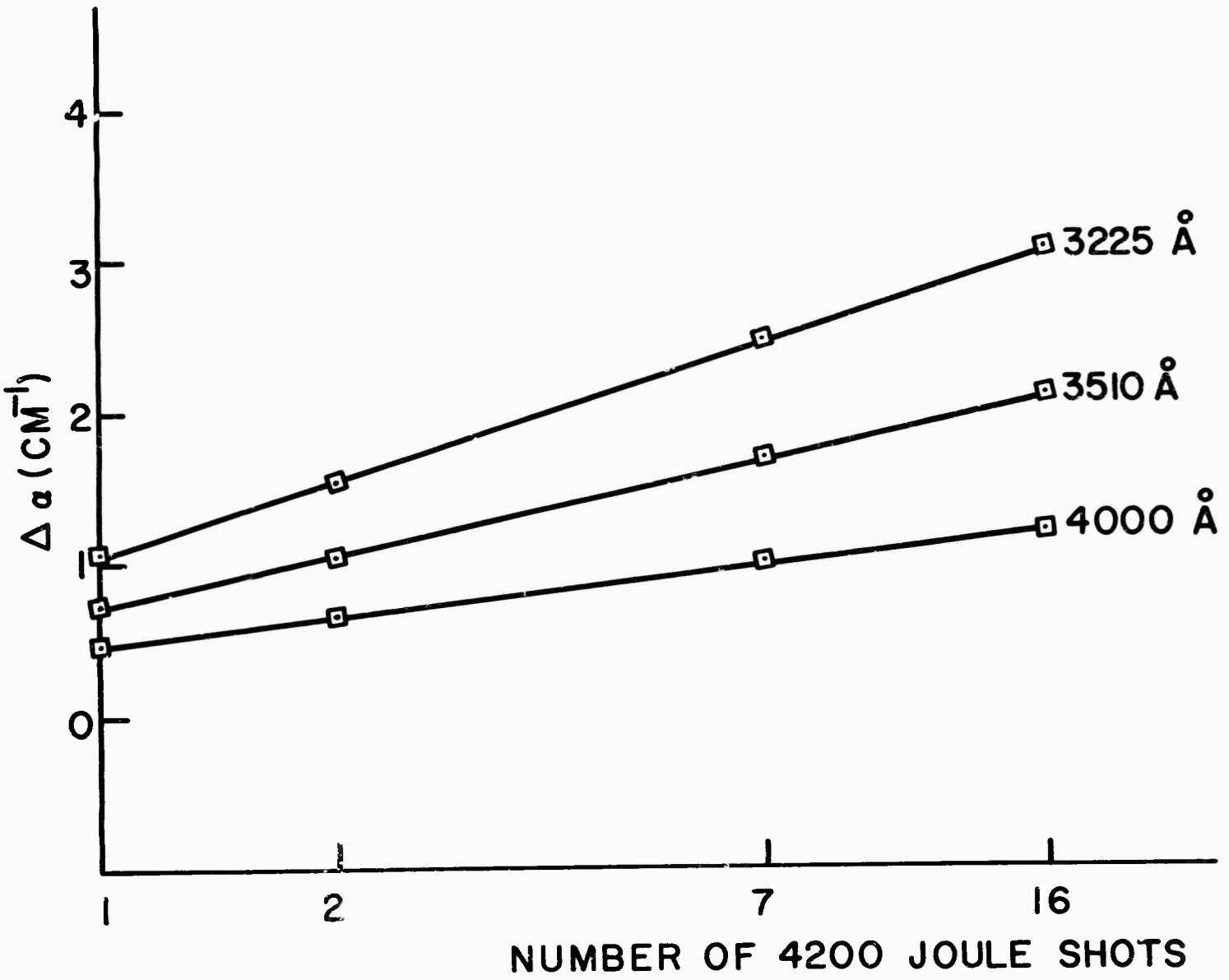

Fig. 2.2

Increase in Optical Absorption after Baking to Remove Previous Solarization. The upper line for the 3225Å data is the optical absorption obtained on the first solarization.

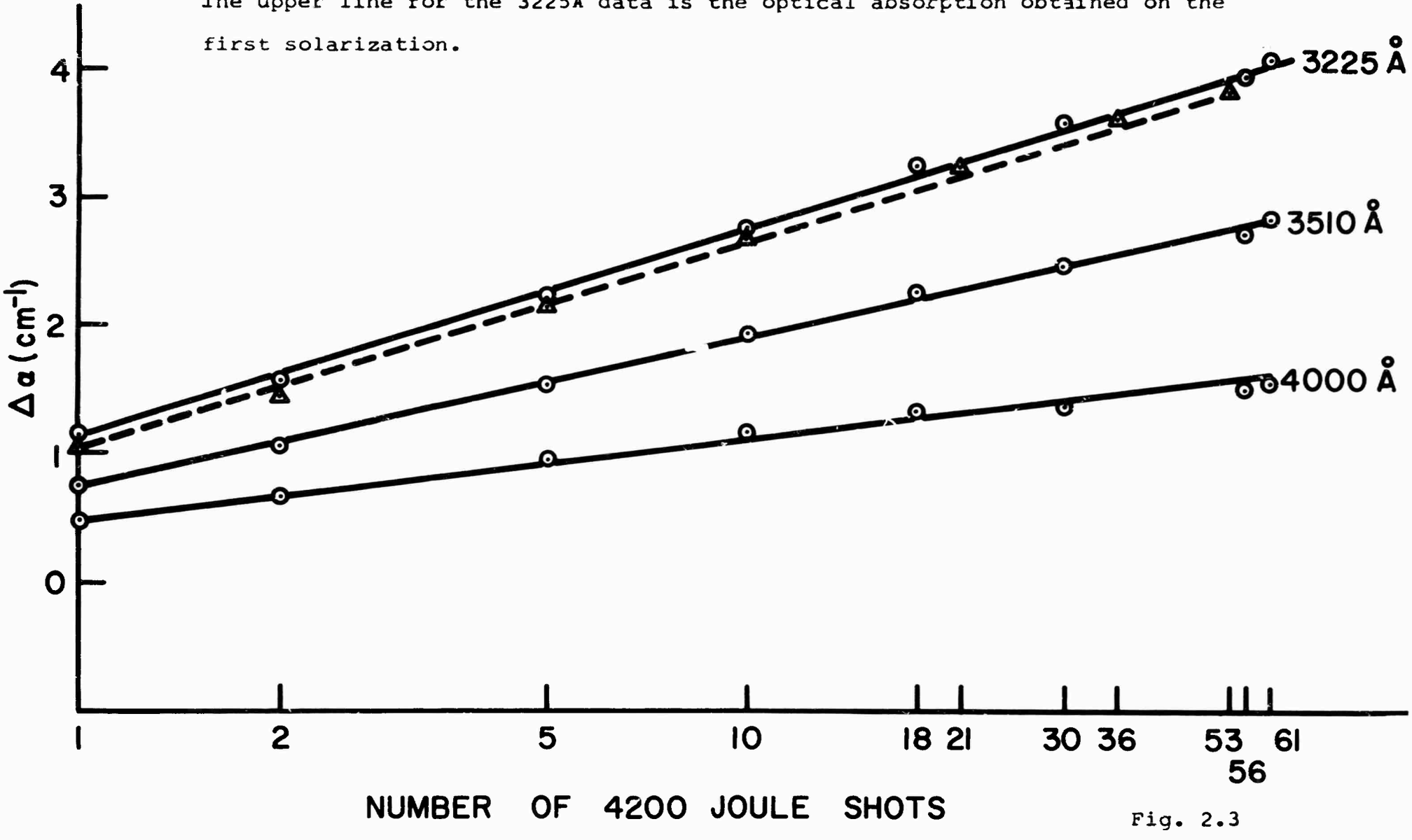

Fig. 2.3

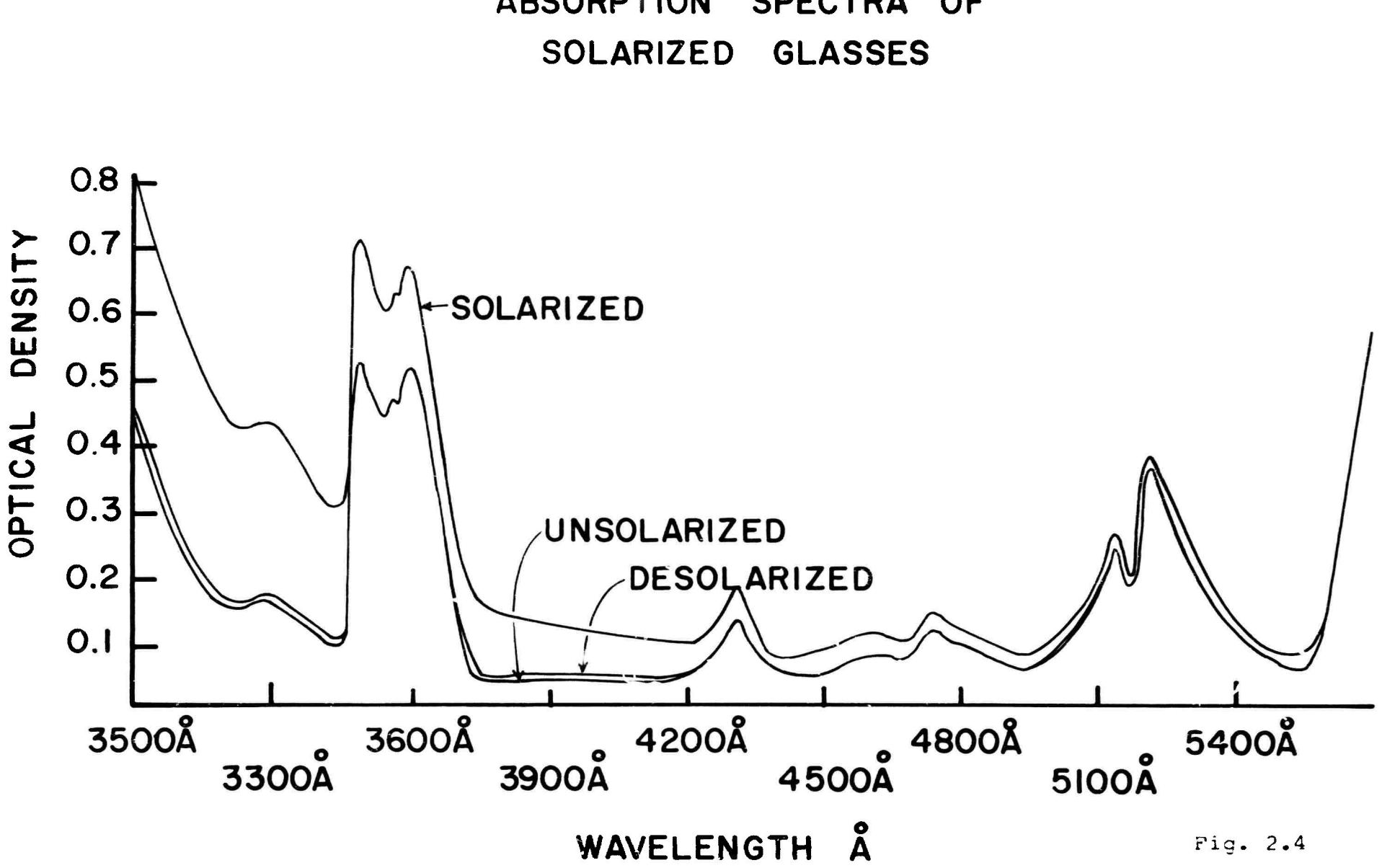
ABSORPTION SPECTRA OF
SOLARIZED GLASSES
OPTICAL DENSITY
0.8
0.7
0.6
0.5
0.4
0.3
0.2
0.1
SOLARIZED
UNSOLARIZED
DESOLARIZED
3500Å
3300Å
3600Å
3900Å
4200Å
4500Å
4800Å
5100Å
5400Å
WAVELENGTH Å

Fig. 2.4

FIG. 2.5

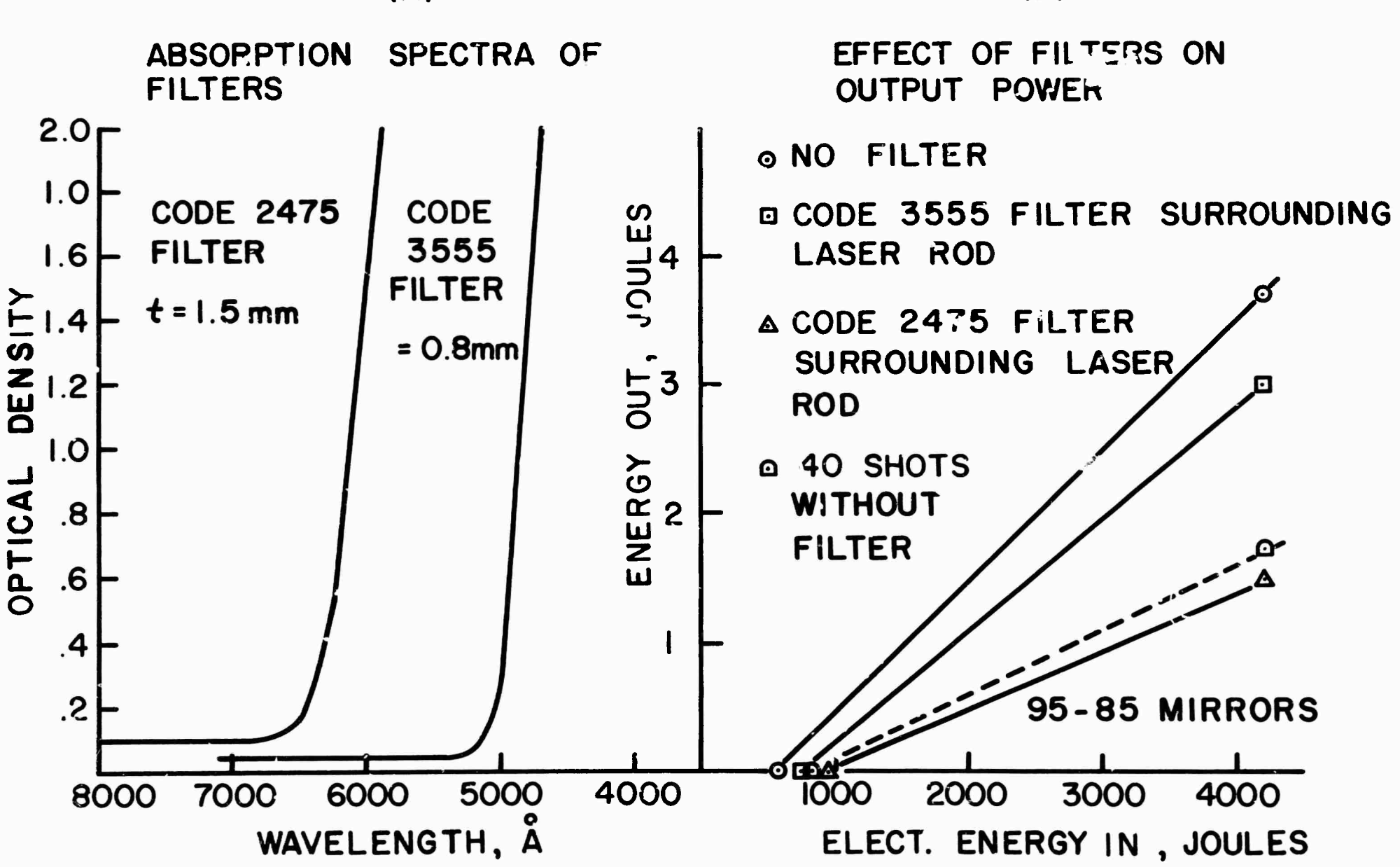
(A)
ABSORPTION SPECTRA OF FILTERS
OPTICAL DENSITY
2.0
1.0
1.6
1.4
1.2
1.0
.8
.6
.4
.2
CODE 2475 FILTER
t = 1.5 mm
CODE 3555 FILTER
= 0.8mm
8000
7000
6000
5000
4000
WAVELENGTH, Å
(B)
EFFECT OF FILTERS ON OUTPUT POWER
NO FILTER
CODE 3555 FILTER SURROUNDING LASER ROD
CODE 2475 FILTER SURROUNDING LASER ROD
40 SHOTS WITHOUT FILTER
95-85 MIRRORS
ENERGY OUT, JOULES
4
3
2
1
1000
2000
3000
4000
ELECT. ENERGY IN , JOULES

FIG. 2.6

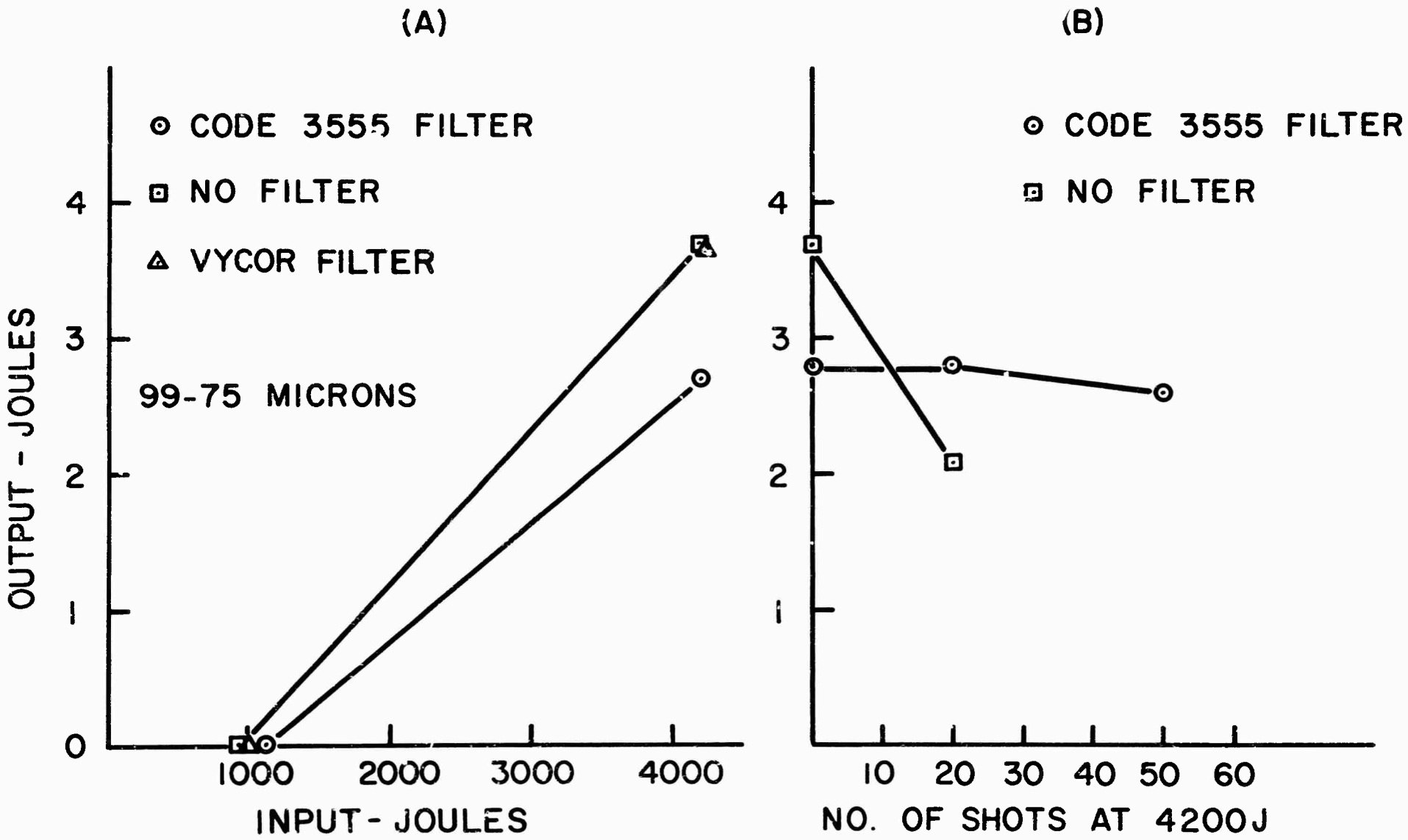
(A)
CODE 3555 FILTER
NO FILTER
VYCOR FILTER
99-75 MICRONS
OUTPUT - JOULES
0
1
2
3
4
1000
2000
3000
4000
INPUT - JOULES
(B)
CODE 3555 FILTER
NO FILTER
1
2
3
4
10
20
30
40
50
60
NO. OF SHOTS AT 4200J

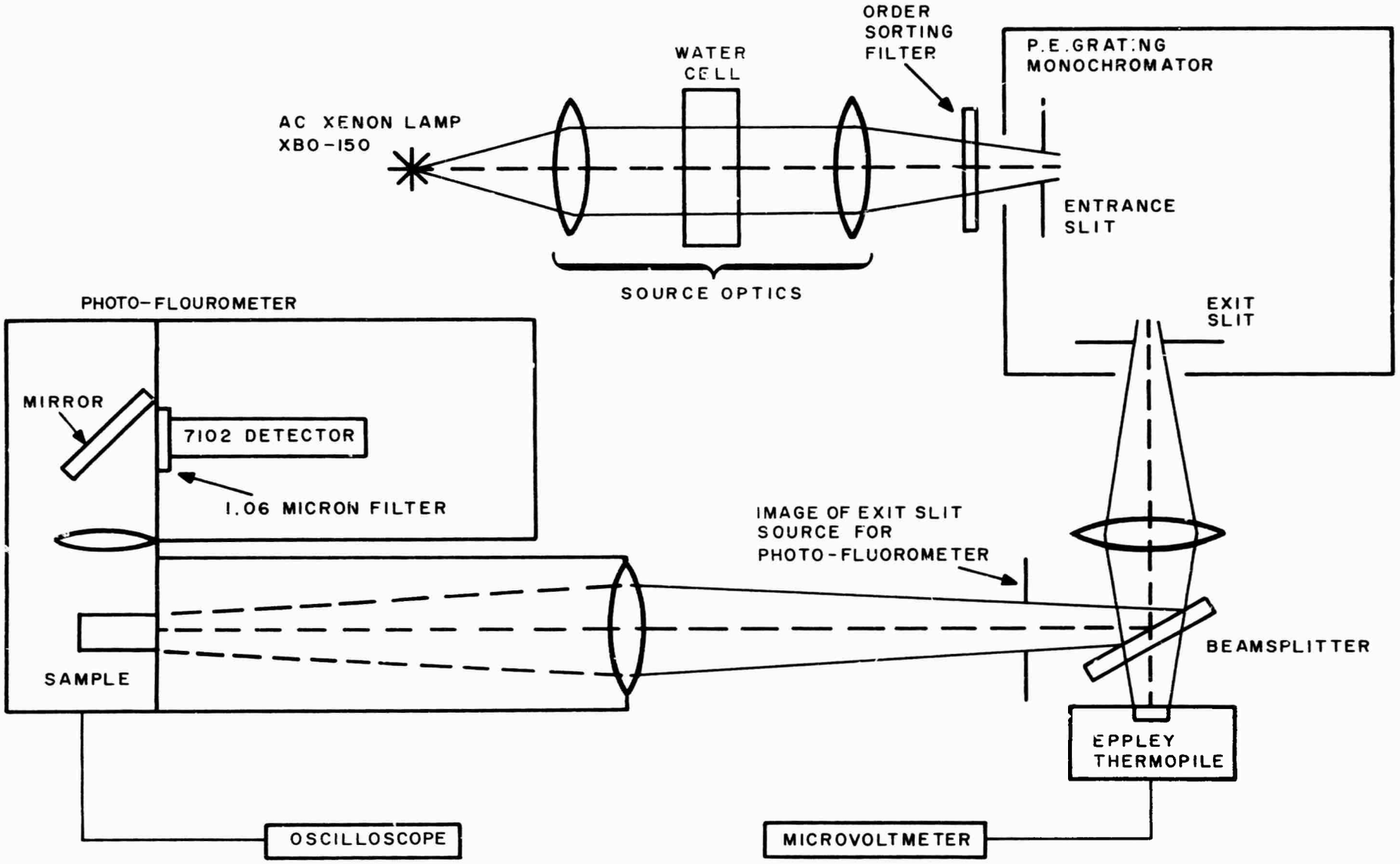

DIAGRAM OF SPECTRAL PUMPING EFFICIENCY EXPERIMENT Fig. 3.1

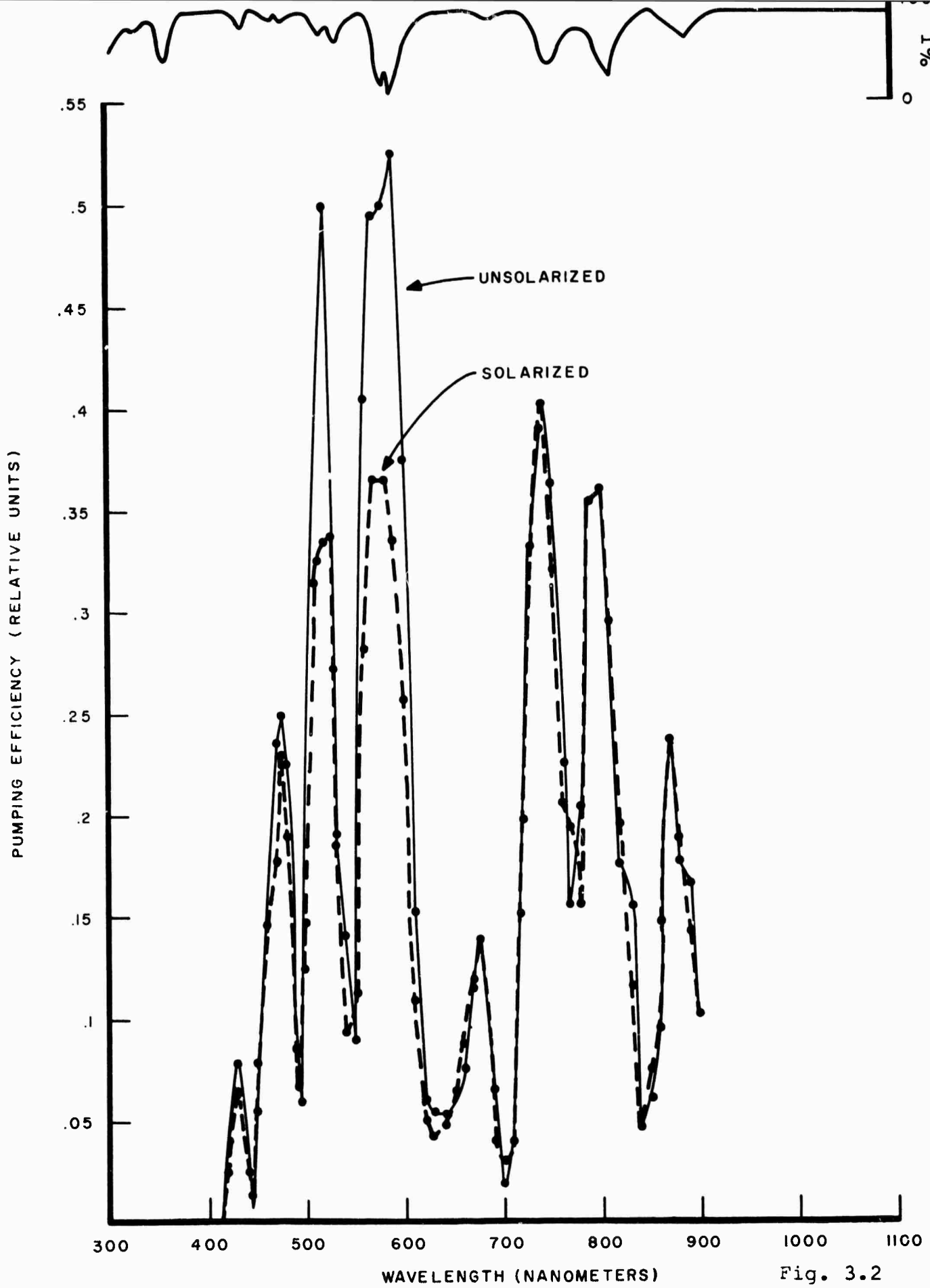

Fig. 3.2

SPECTRAL PUMPING EFFICIENCY OF SOLARIZED AND UNSOLARIZED CORNING CODE 0580 LASER GLASS--ALSO SHOWN, TRANSMISSION SPECTRUM

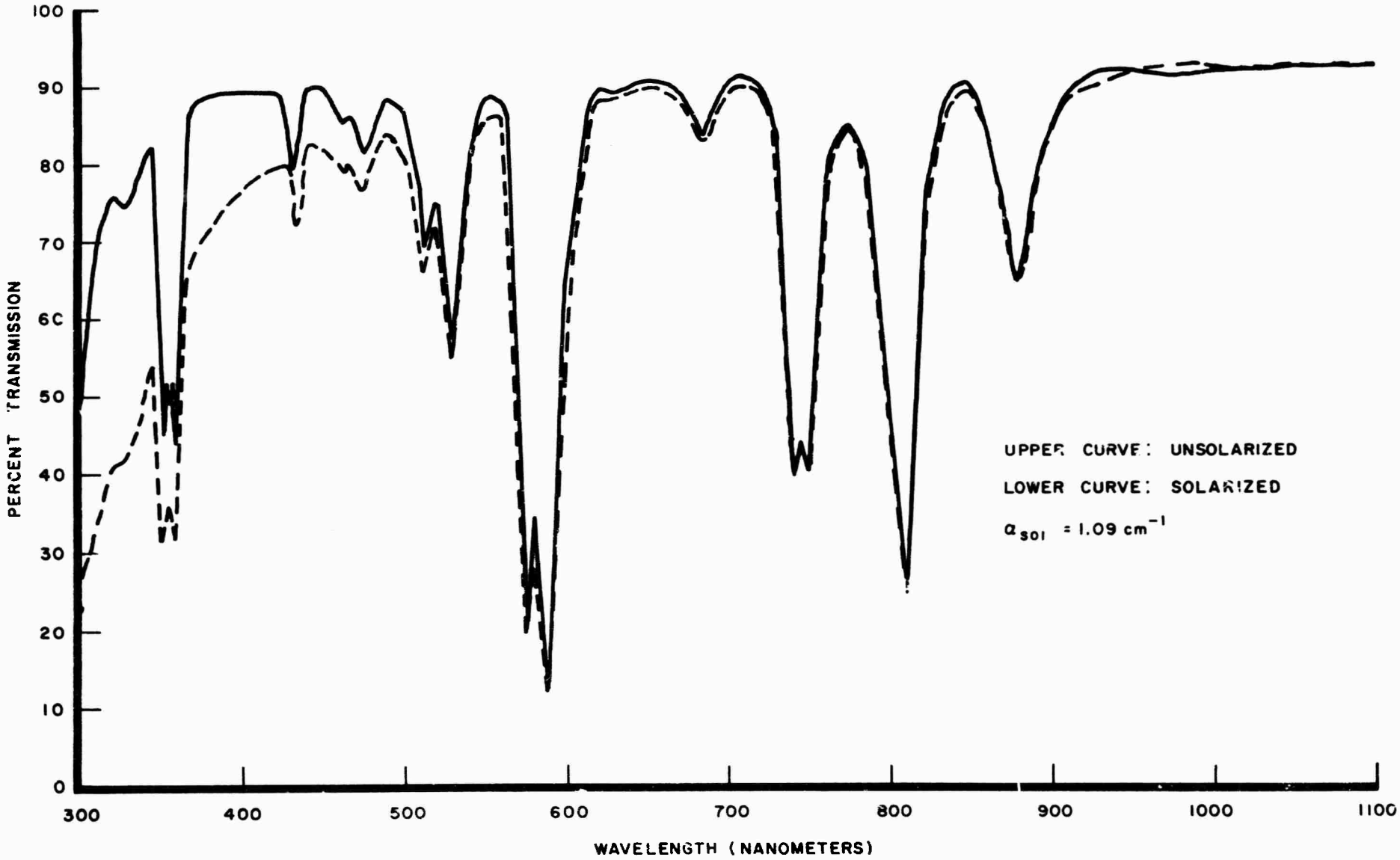

EFFECT OF SOLARIZATION ON SPECTRAL TRANSMISSION OF LASER GLASS Fig. 3.3

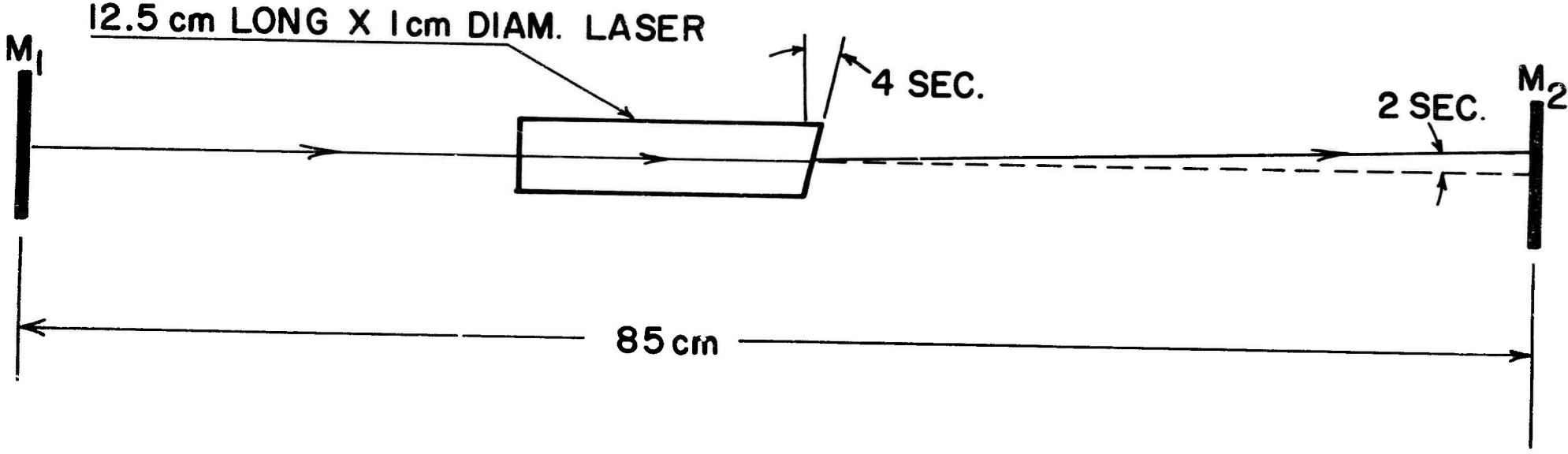

FIG. 4.1 DETAILS OF OPTICAL ALIGNMENT OF LASER CAVITY

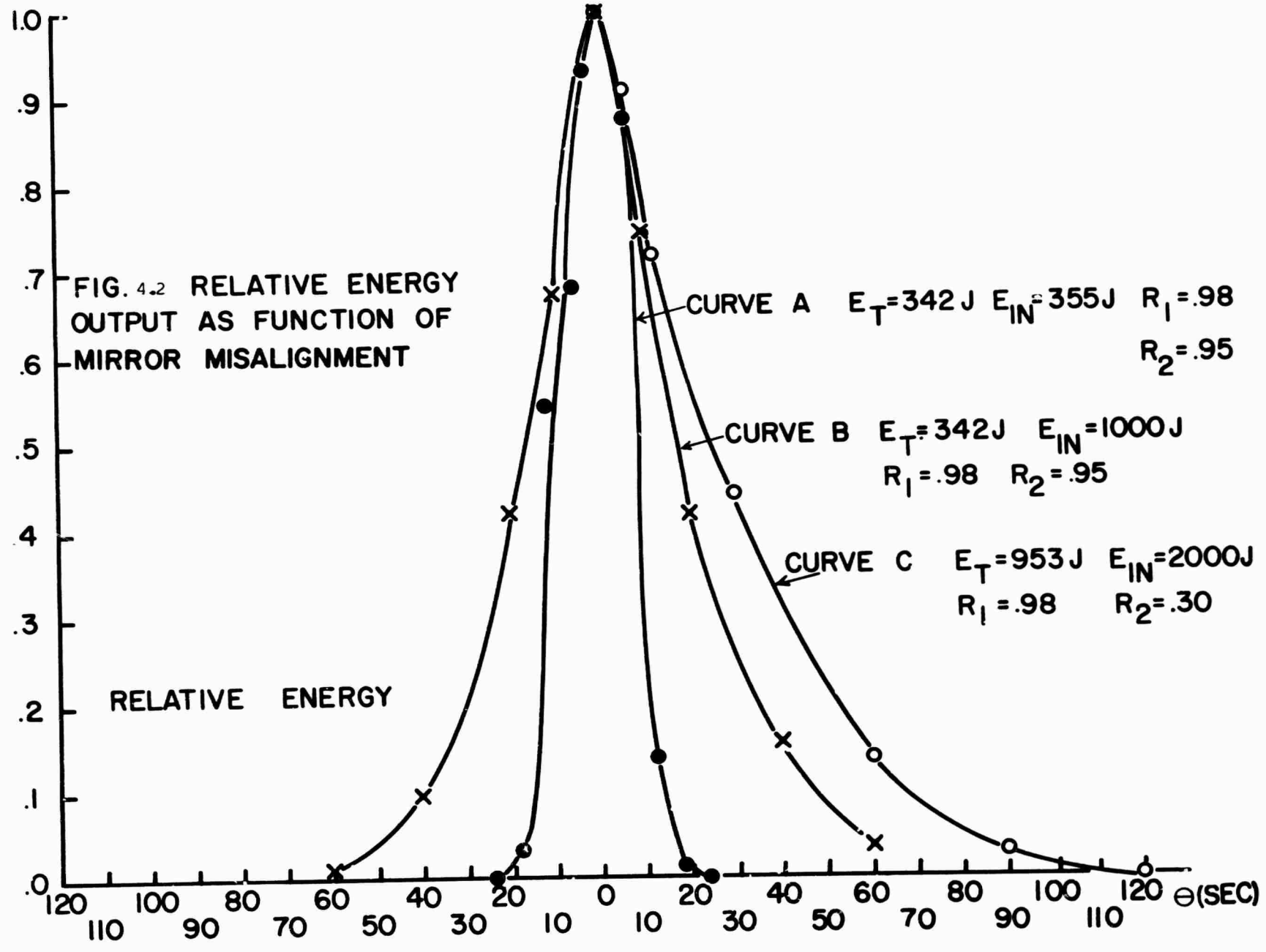

FIG. 4.2 RELATIVE ENERGY OUTPUT AS FUNCTION OF MIRROR MISALIGNMENT

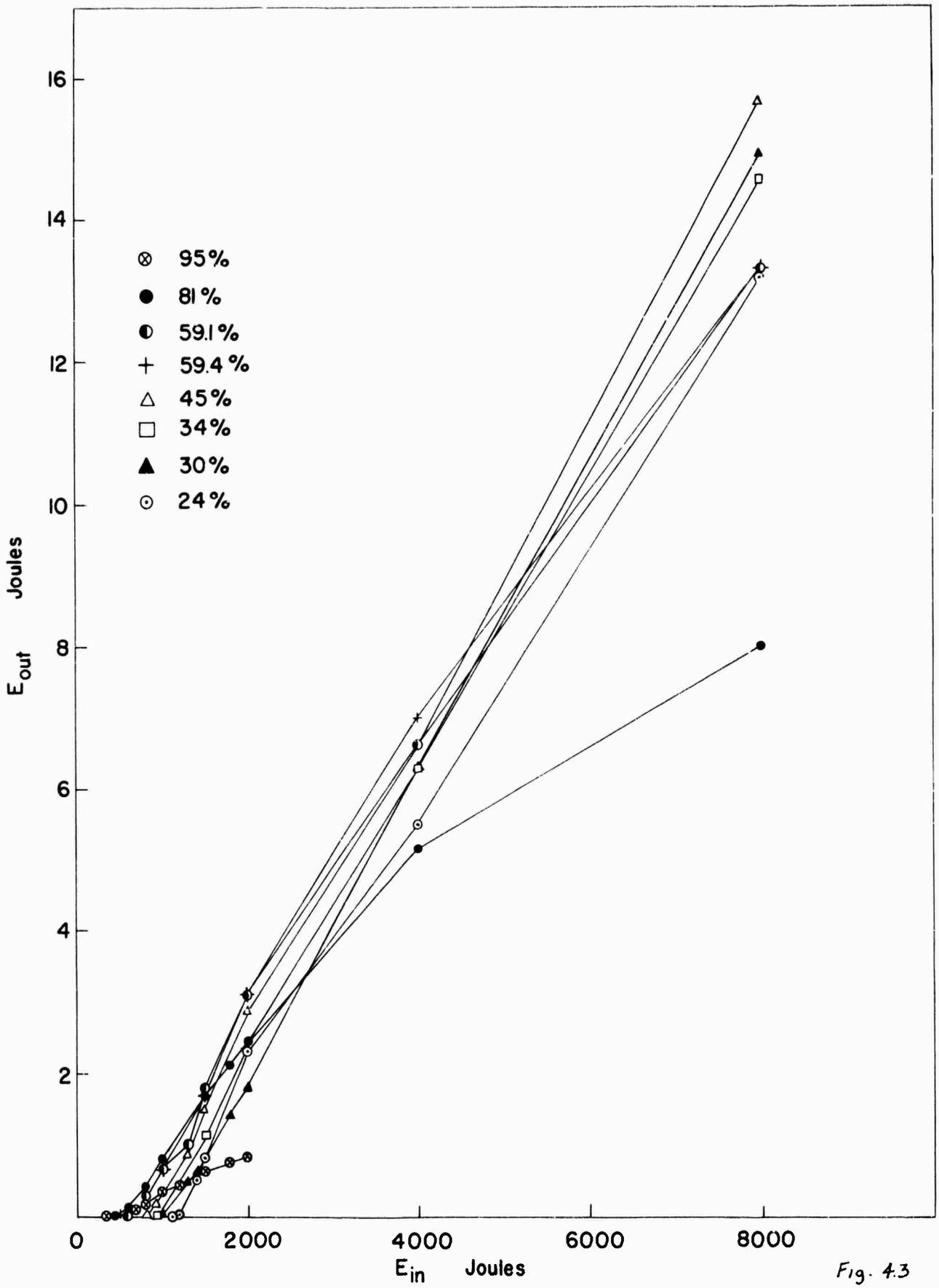
16
14
12
10
8
6
4
2
0
2000
4000
6000
8000
E_{out} Joules
E_{in} Joules
95%
81%
59.1%
59.4%
45%
34%
30%
24%

Fig. 4.3

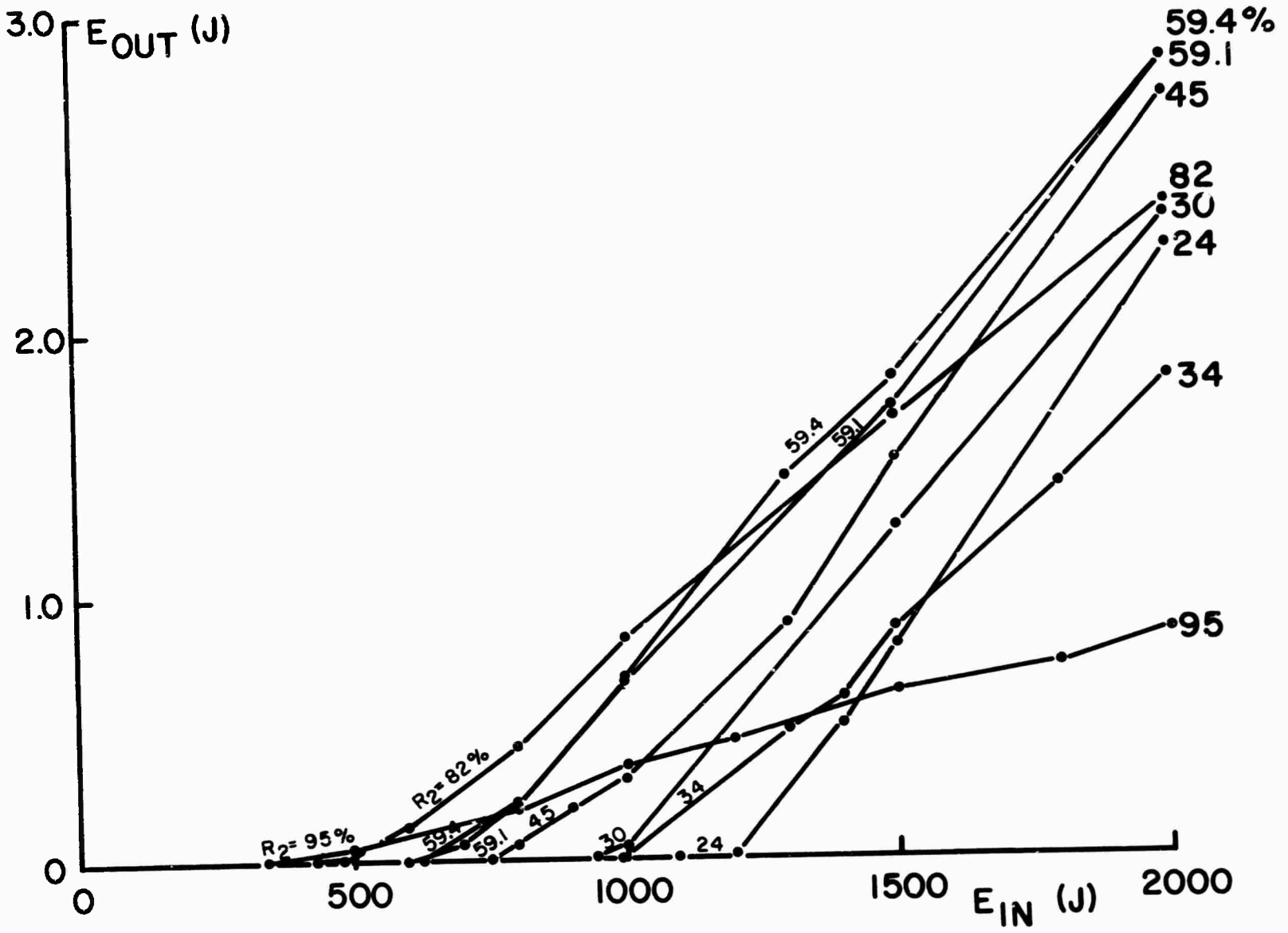

FIG. 4.4 OUTPUT ENERGY VERSUS INPUT ELECTRICAL ENERGY FOR GIVEN VALUES OF OUTPUT MIRROR REFLECTANCE. $E_{IN} \leq 2000$ J

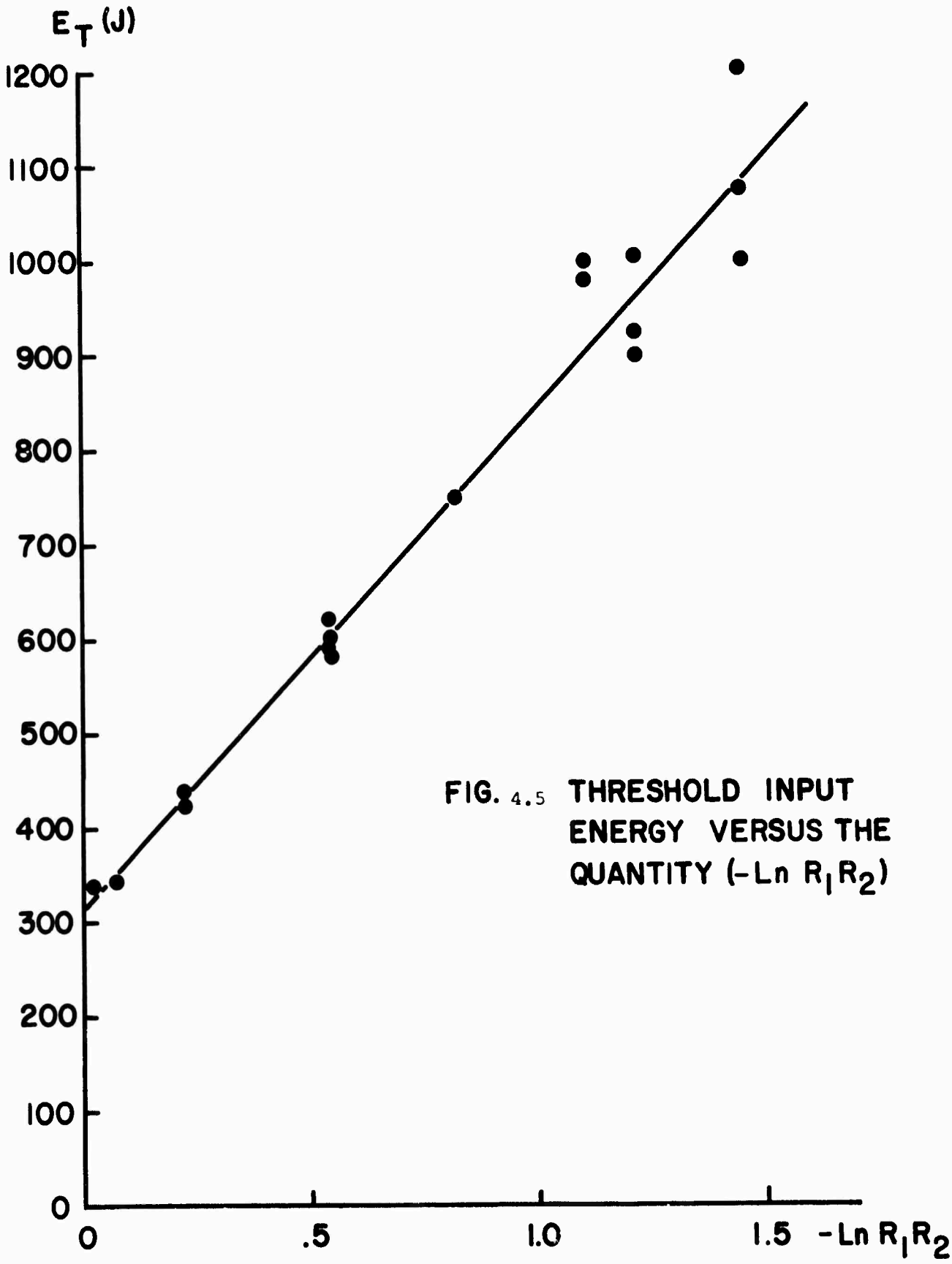

FIG. 4.5 THRESHOLD INPUT ENERGY VERSUS THE QUANTITY (-Ln R_1R_2)

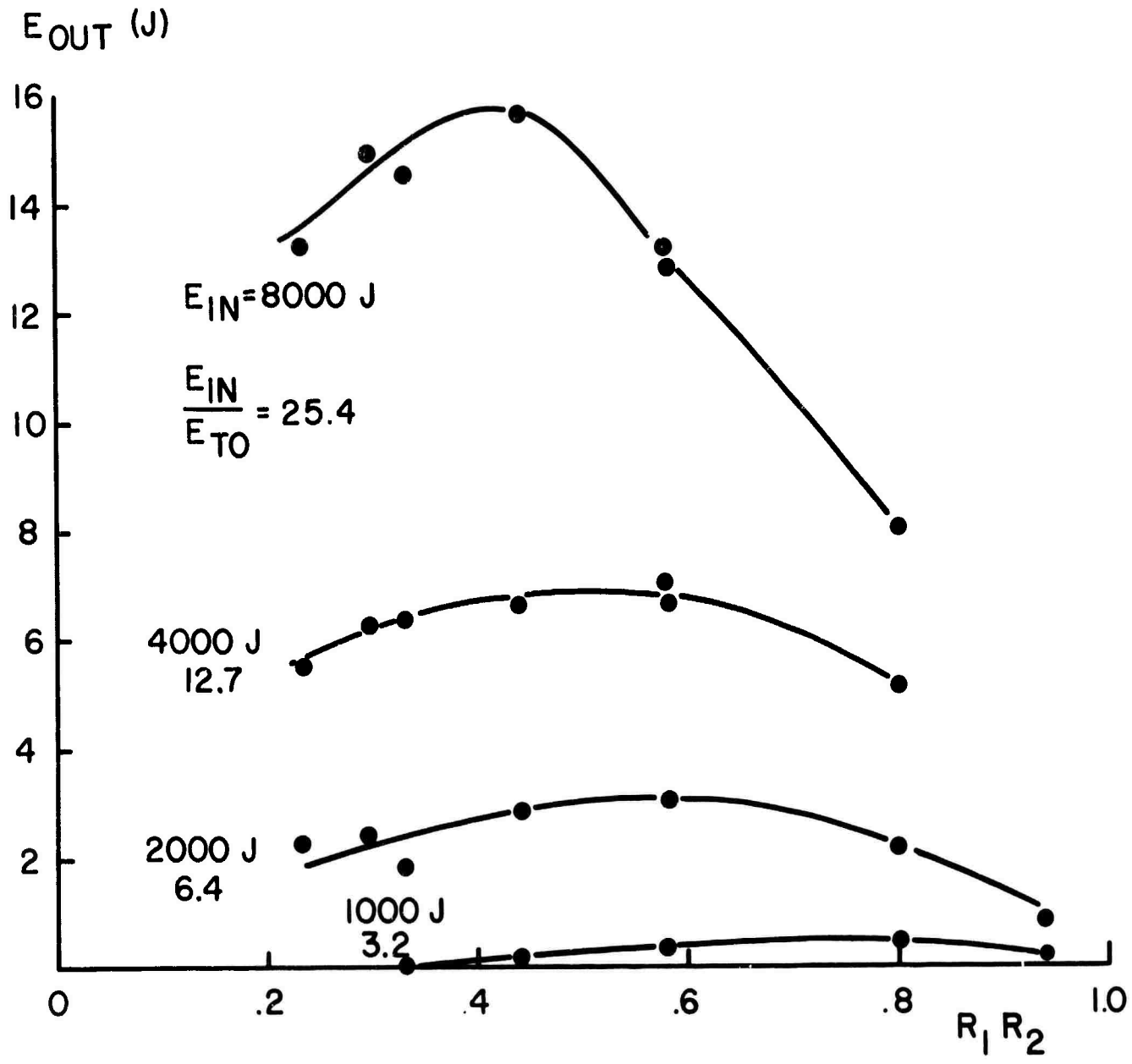

FIG. 4.6 OUTPUT ENERGY VERSUS $R_1 R_2$ FOR DIFFERENT LEVELS OF EXCITATION. IN ALL CASES $R_1 = 0.982$

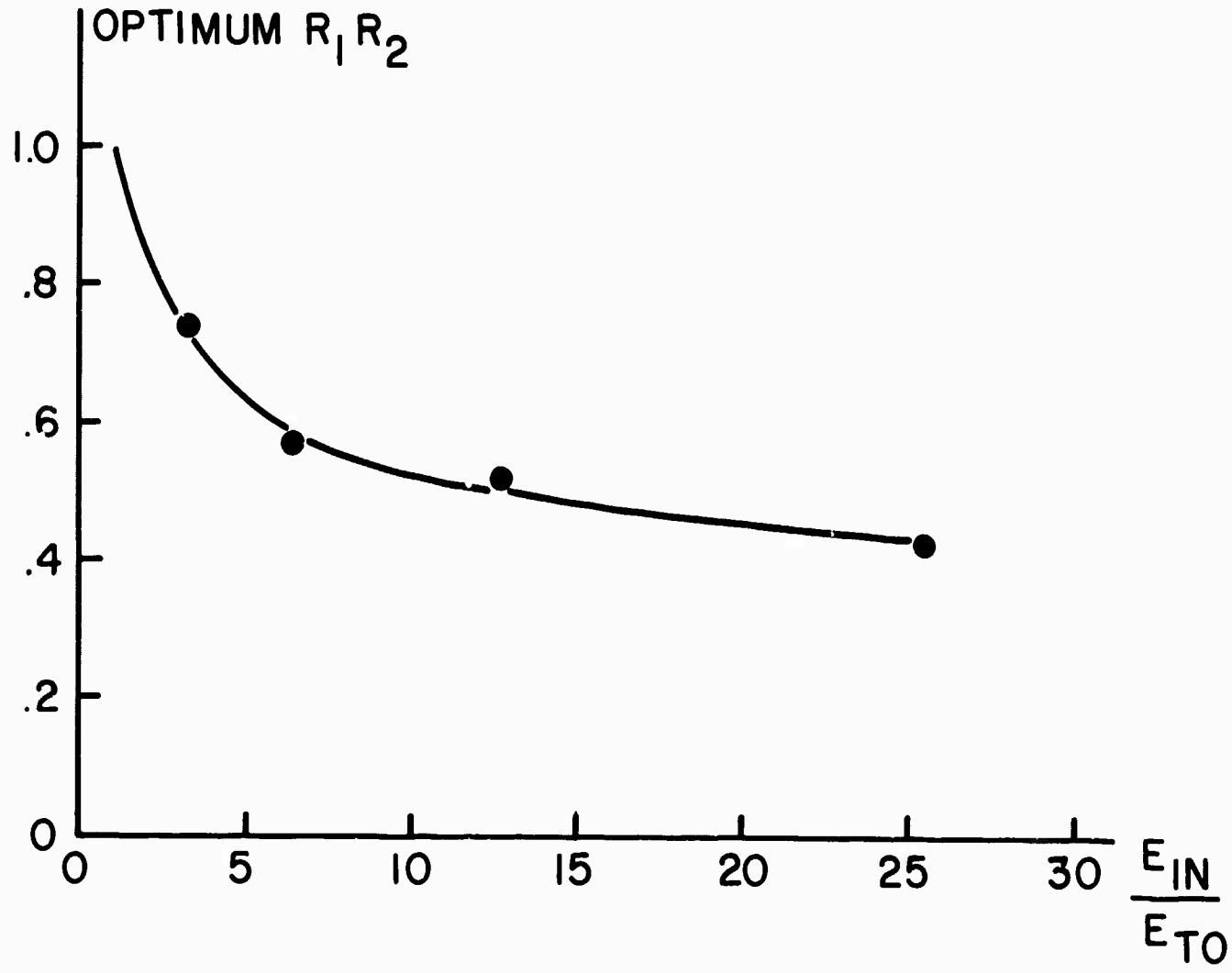

FIG. 4.7 OPTIMUM $R_1 R_2$ FOR MAXIMUM ENERGY OUTPUT AS FUNCTION OF PUMP ENERGY

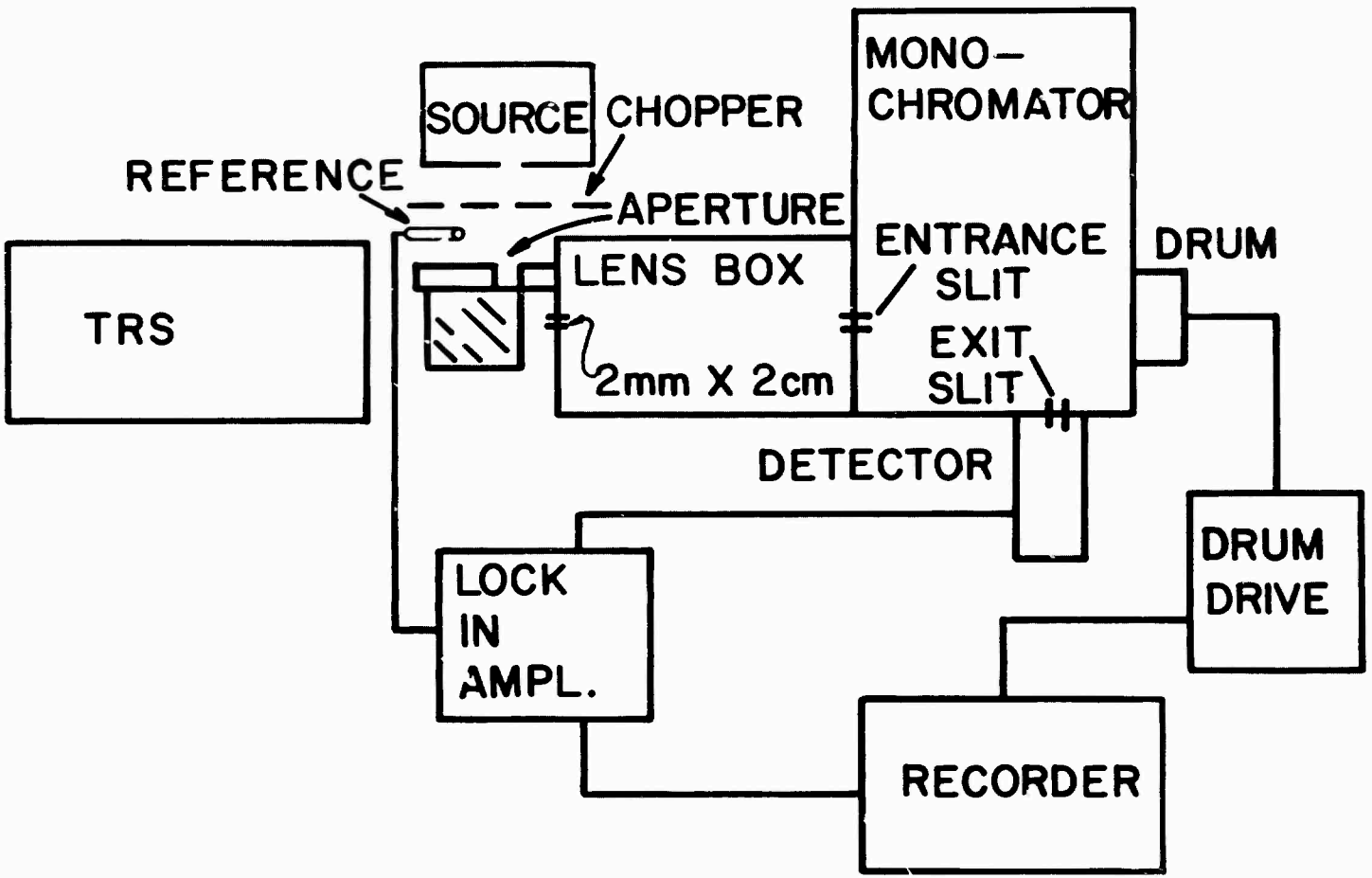

FLUORESCENCE APPARATUS

Fig. 5.2

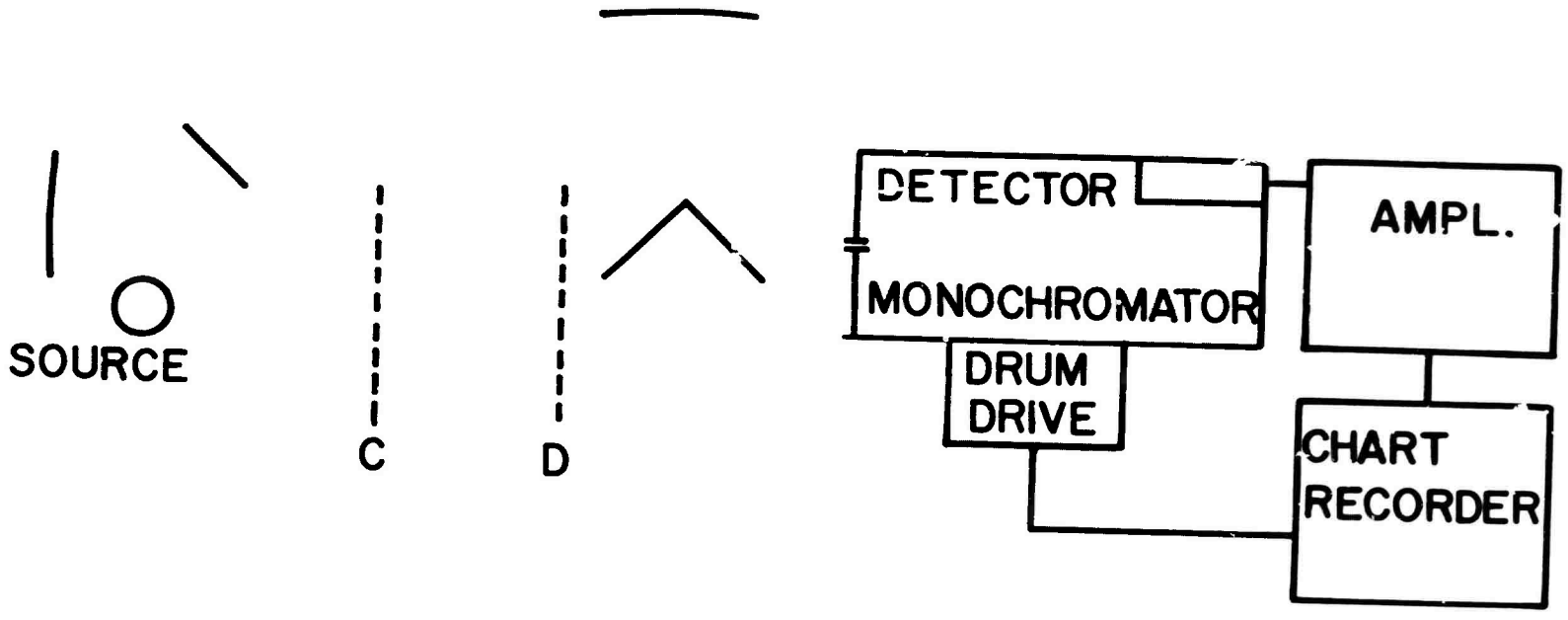

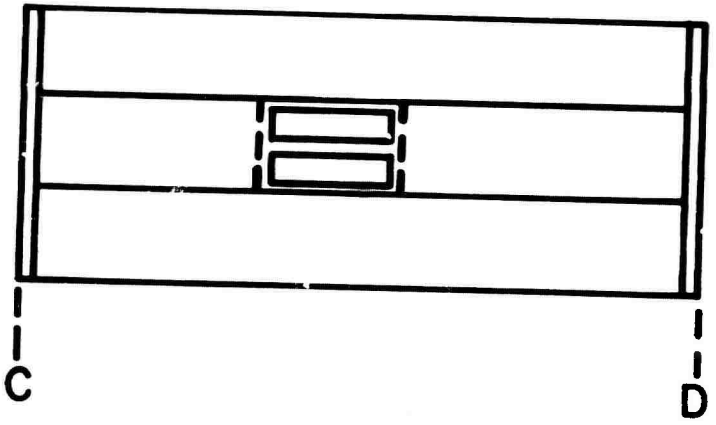

ABSORPTION APPARATUS

Fig. 5.3

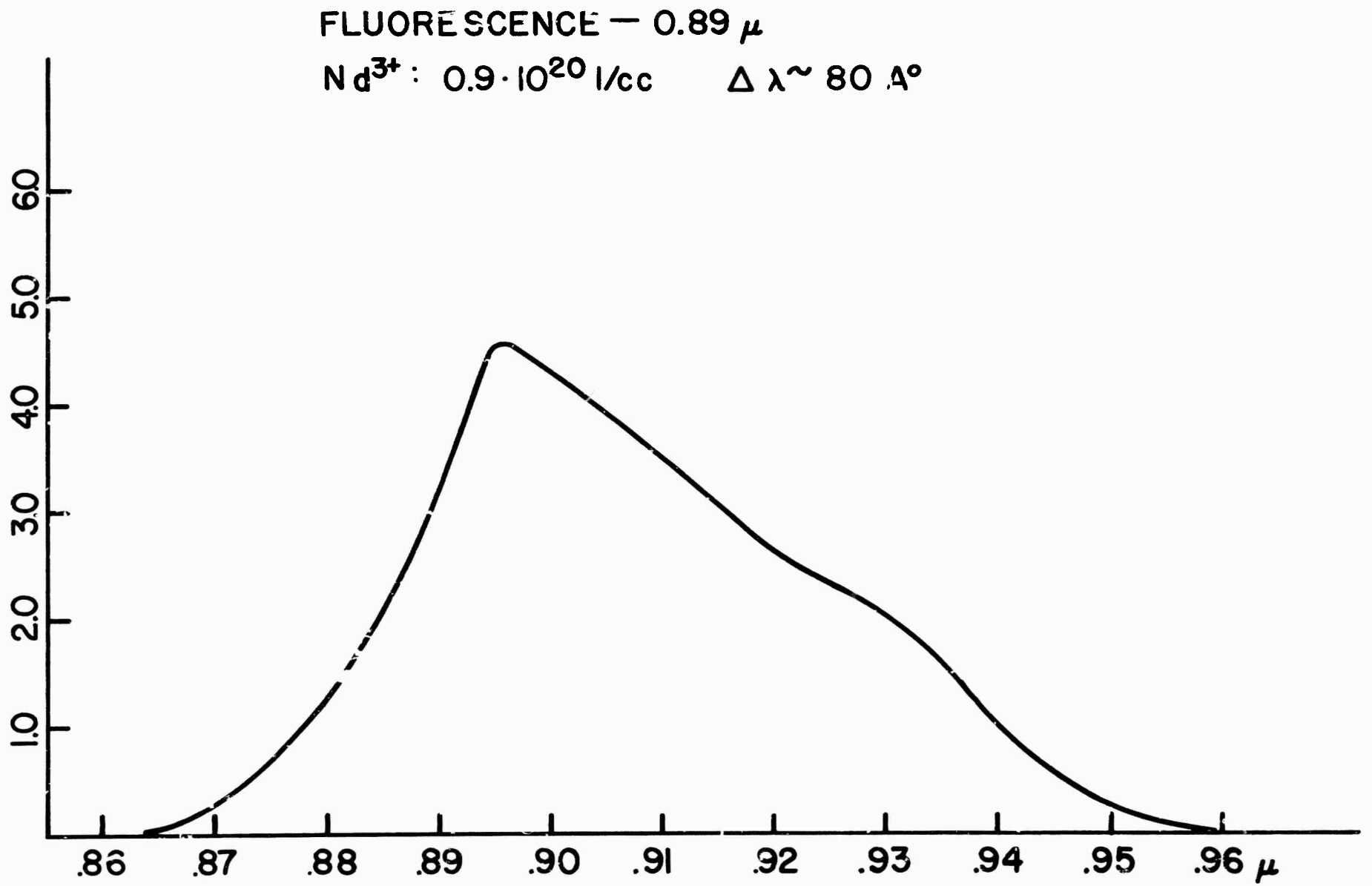
FLUORESCENCE — 0.89 μ
Nd3+ : 0.9·10^20 l/cc
Δ λ~ 80 A°
1.0
2.0
3.0
4.0
5.0
6.0
.86
.87
.88
.89
.90
.91
.92
.93
.94
.95
.96 μ

Fig. 5.4

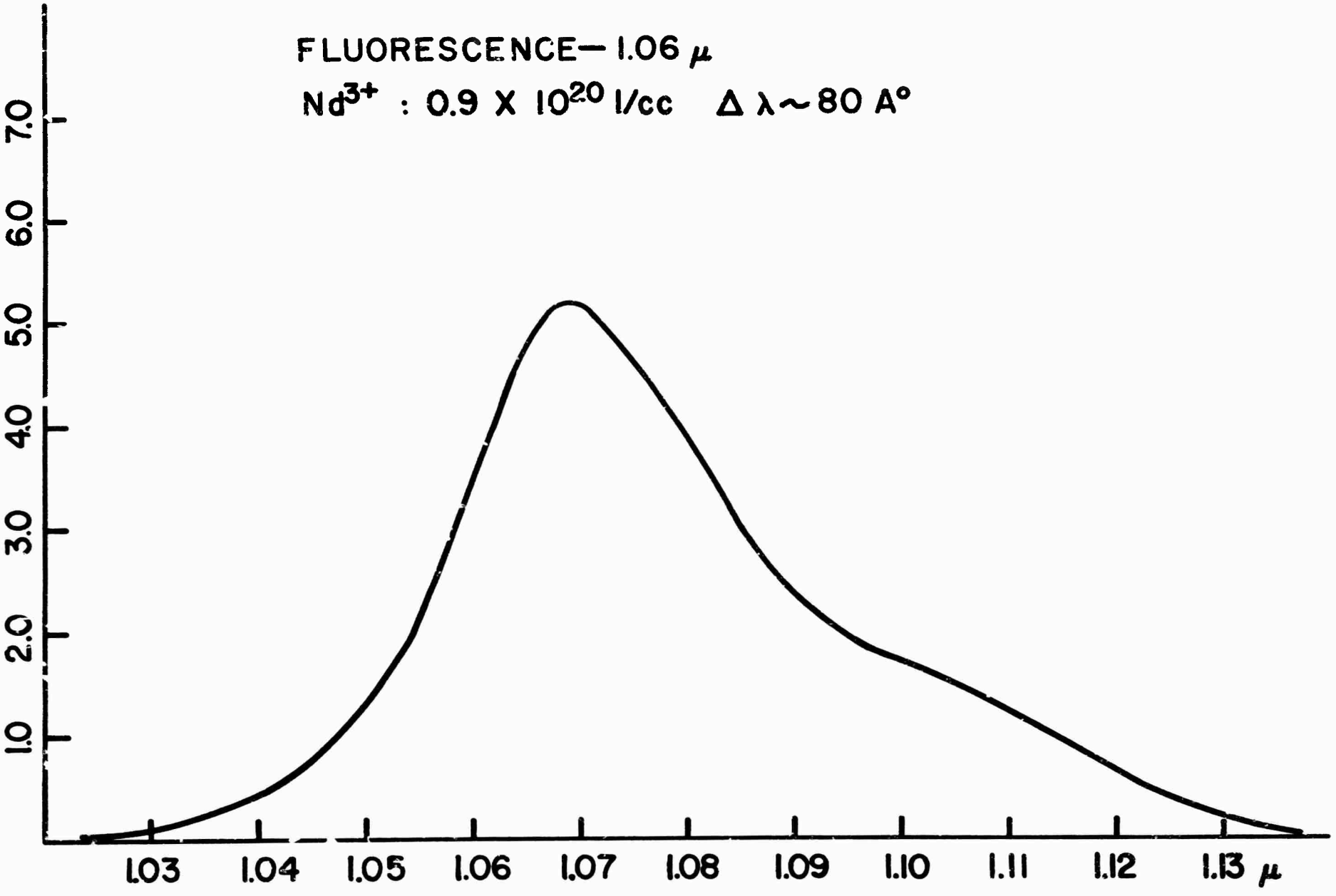
FLUORESCENCE— 1.06 μ
Nd3+ : 0.9 X 10^20 I/cc Δ λ ~ 80 A°
7.0
6.0
5.0
4.0
3.0
2.0
1.0
1.03
1.04
1.05
1.06
1.07
1.08
1.09
1.10
1.11
1.12
1.13 μ

Fig. 5.5

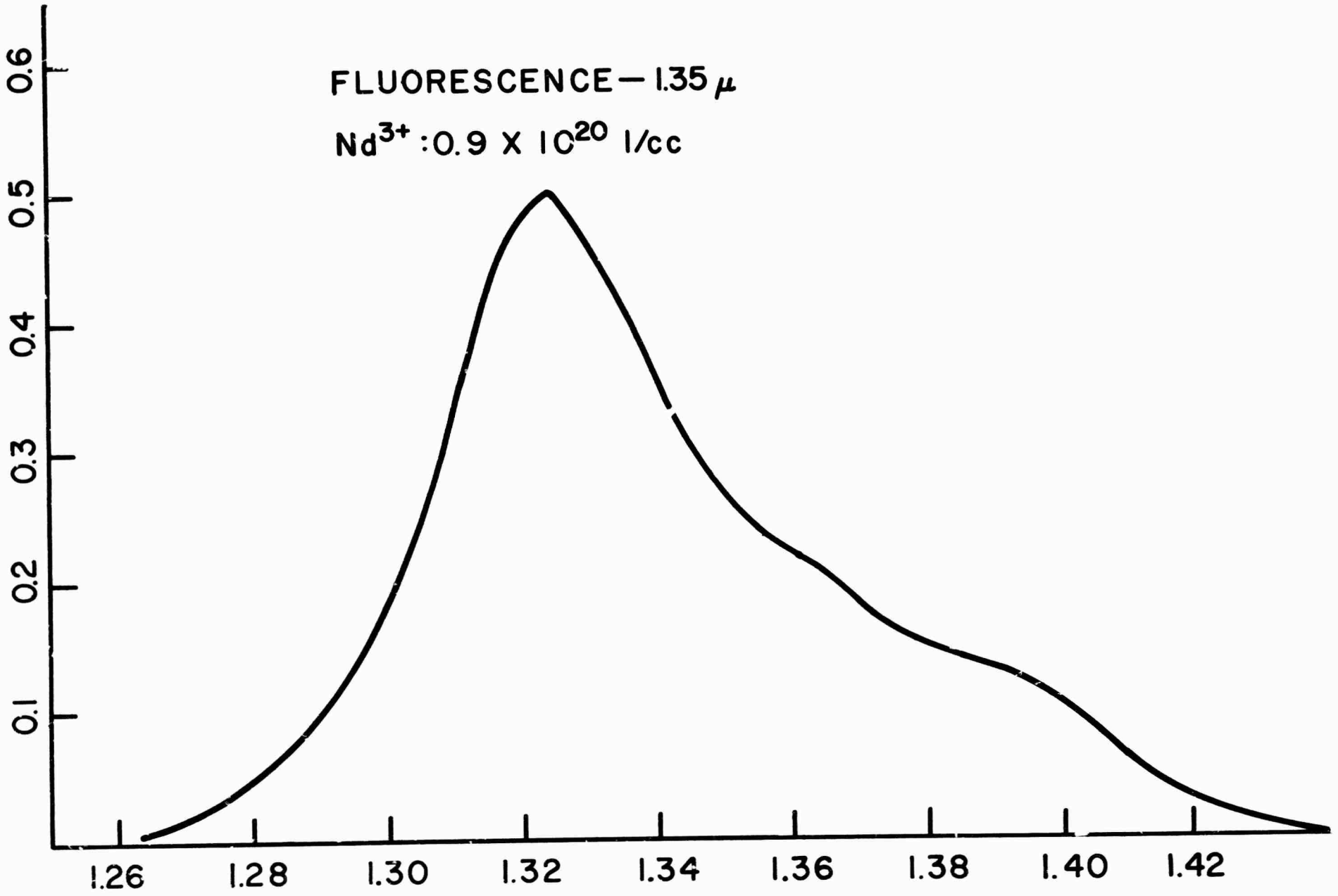
FLUORESCENCE — 1.35 μ
Nd3+ :0.9 X 10^20 1/cc
0.6
0.5
0.4
0.3
0.2
0.1
1.26
1.28
1.30
1.32
1.34
1.36
1.38
1.40
1.42

Fig. 5.6

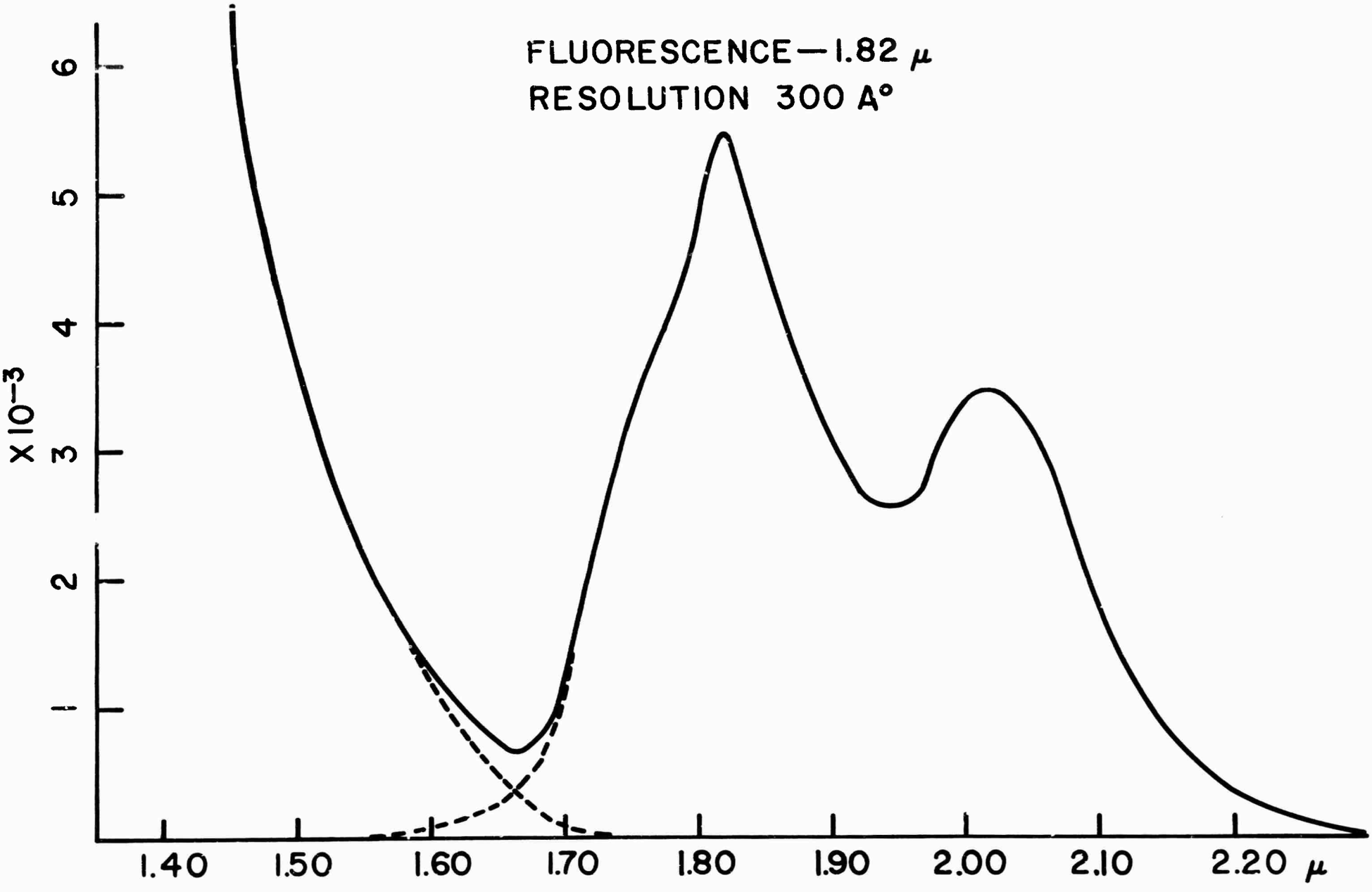
FLUORESCENCE—1.82 μ
RESOLUTION 300 A°
X 10⁻³
1
2
3
4
5
6
1.40
1.50
1.60
1.70
1.80
1.90
2.00
2.10
2.20 μ

Fig. 5.7

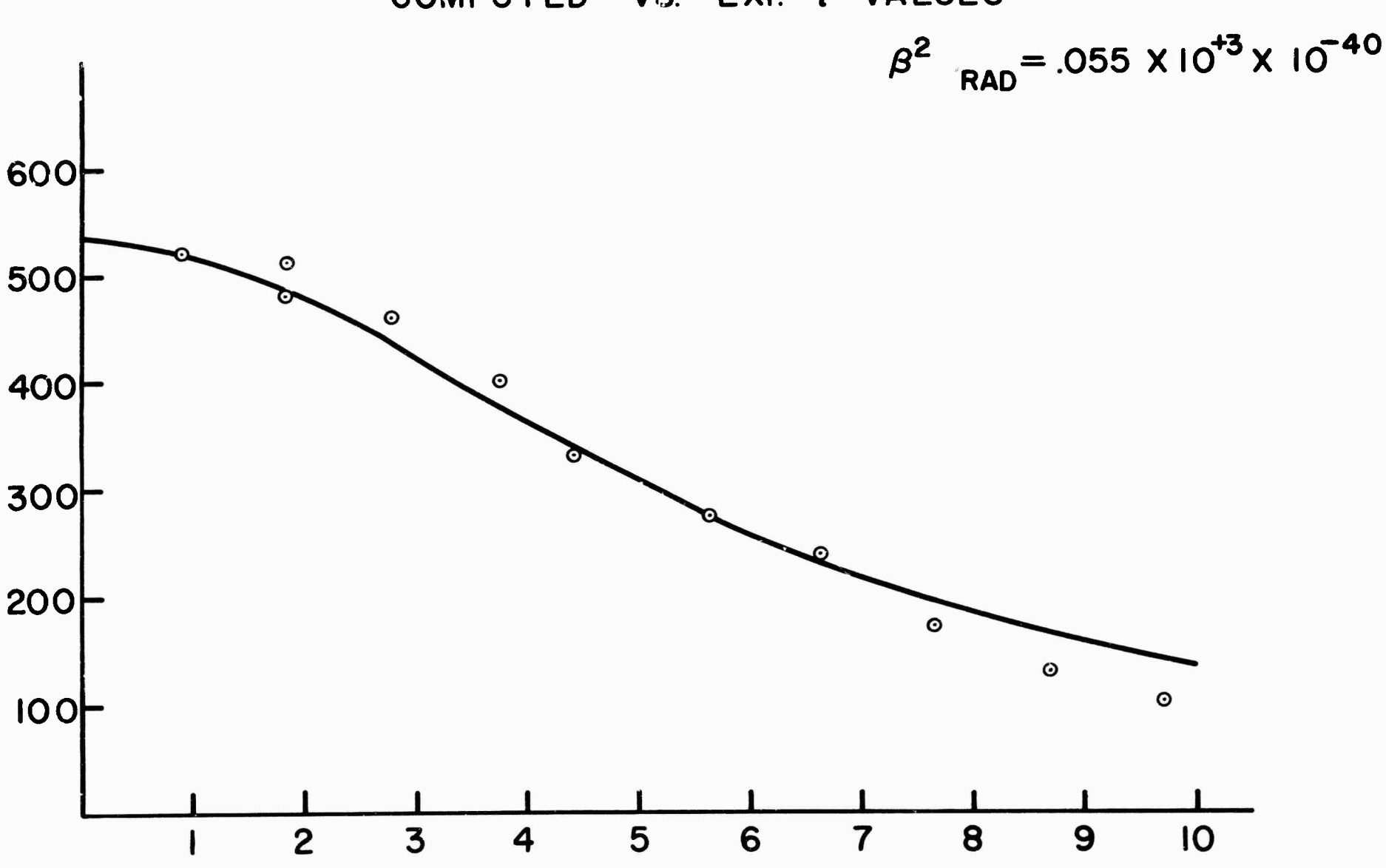
COMPUTED VS. EXP. τ VALUES
$\beta^2_{RAD} = .055 \times 10^{+3} \times 10^{-40}$
600
500
400
300
200
100
1
2
3
4
5
6
7
8
9
10

Fig. 5.8

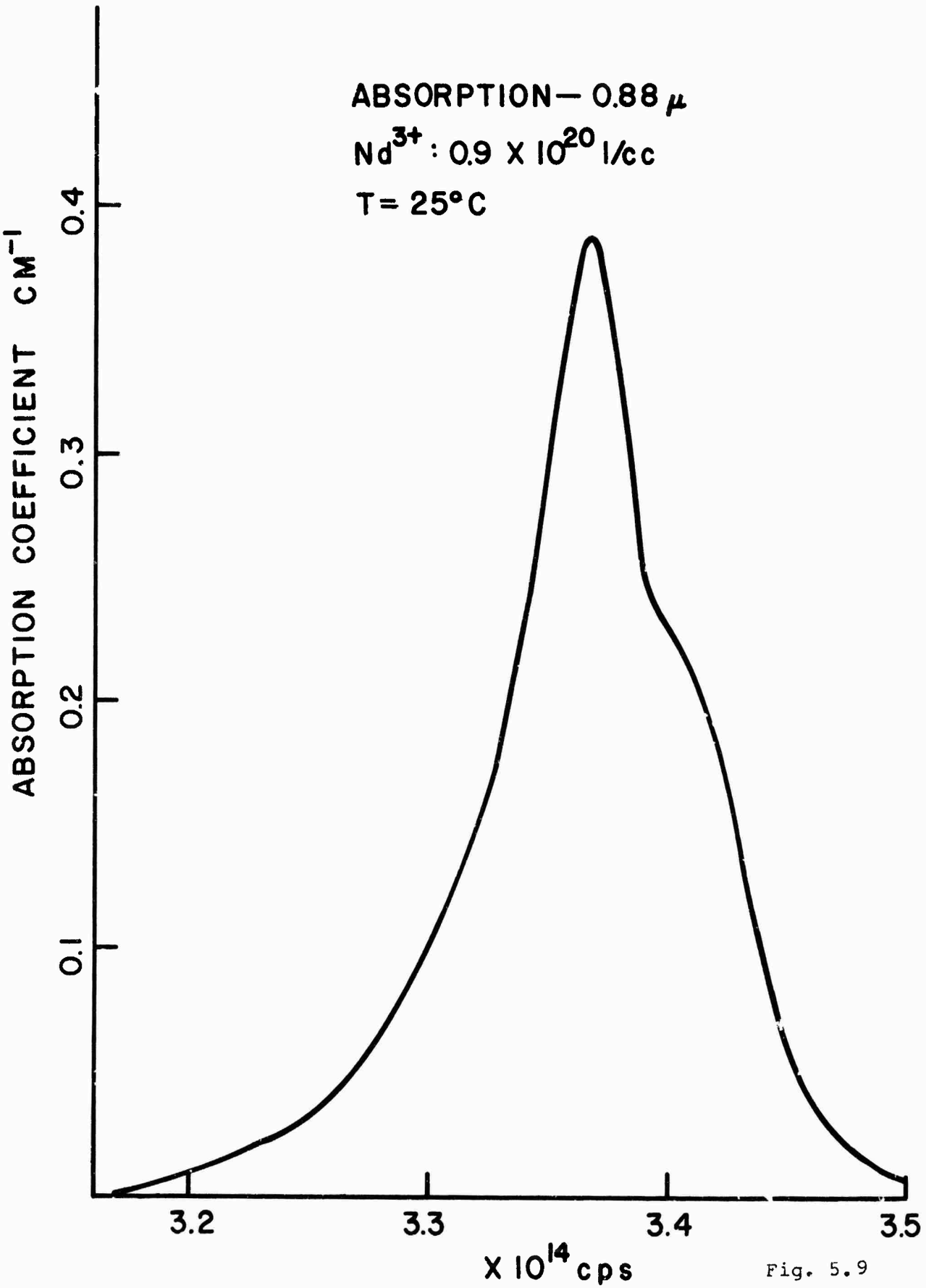
ABSORPTION— 0.88 μ
Nd3+ : 0.9 X 10^20 I/cc
T= 25°C
ABSORPTION COEFFICIENT CM-1
0.1
0.2
0.3
0.4
3.2
3.3
3.4
3.5
X 10^14 cps

Fig. 5.9

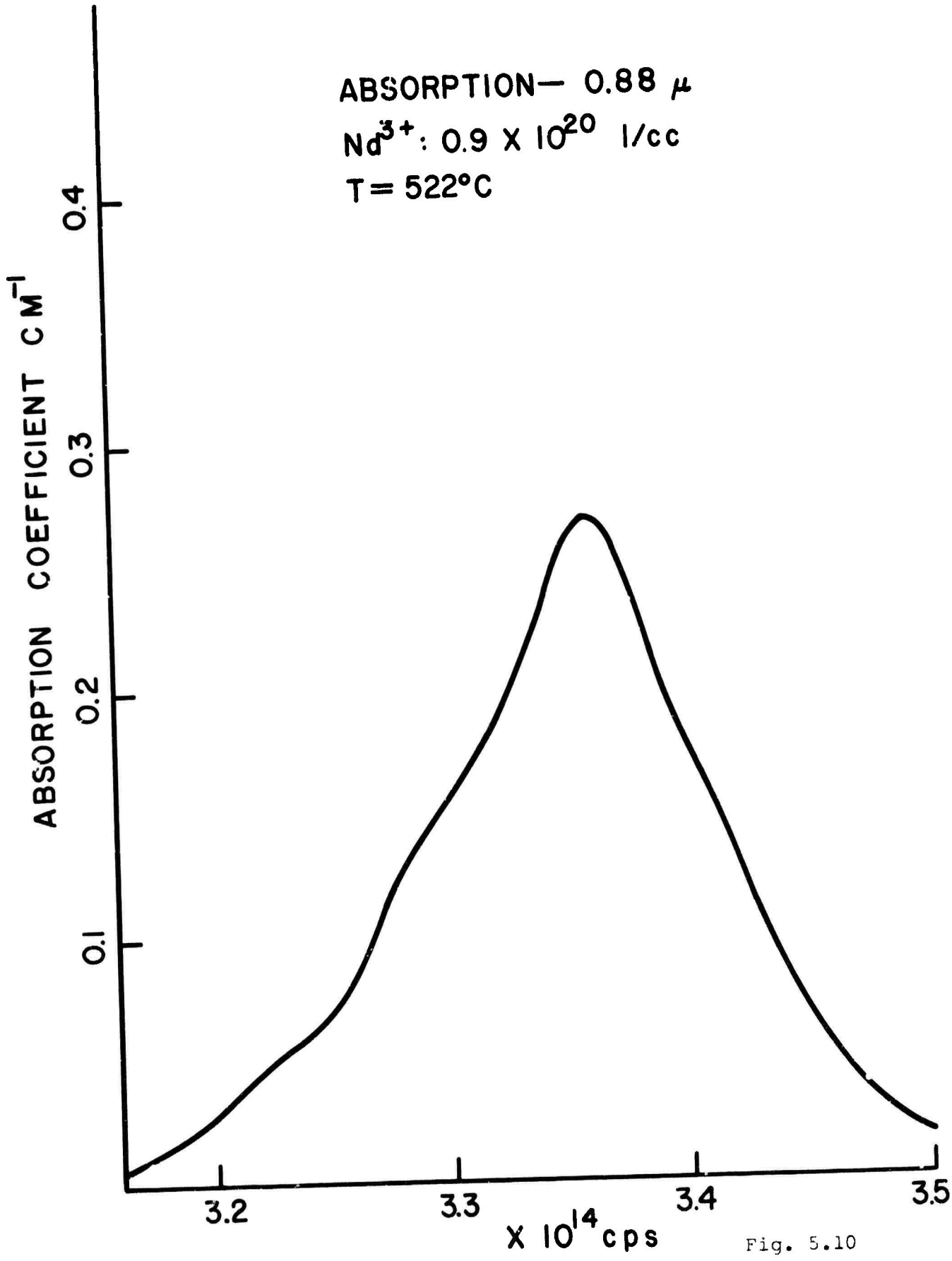
ABSORPTION— 0.88 μ
Nd3+: 0.9 X 10^20 1/cc
T= 522°C
ABSORPTION COEFFICIENT CM-1
0.4
0.3
0.2
0.1
3.2
3.3
3.4
3.5
X 10^14 cps

Fig. 5.10

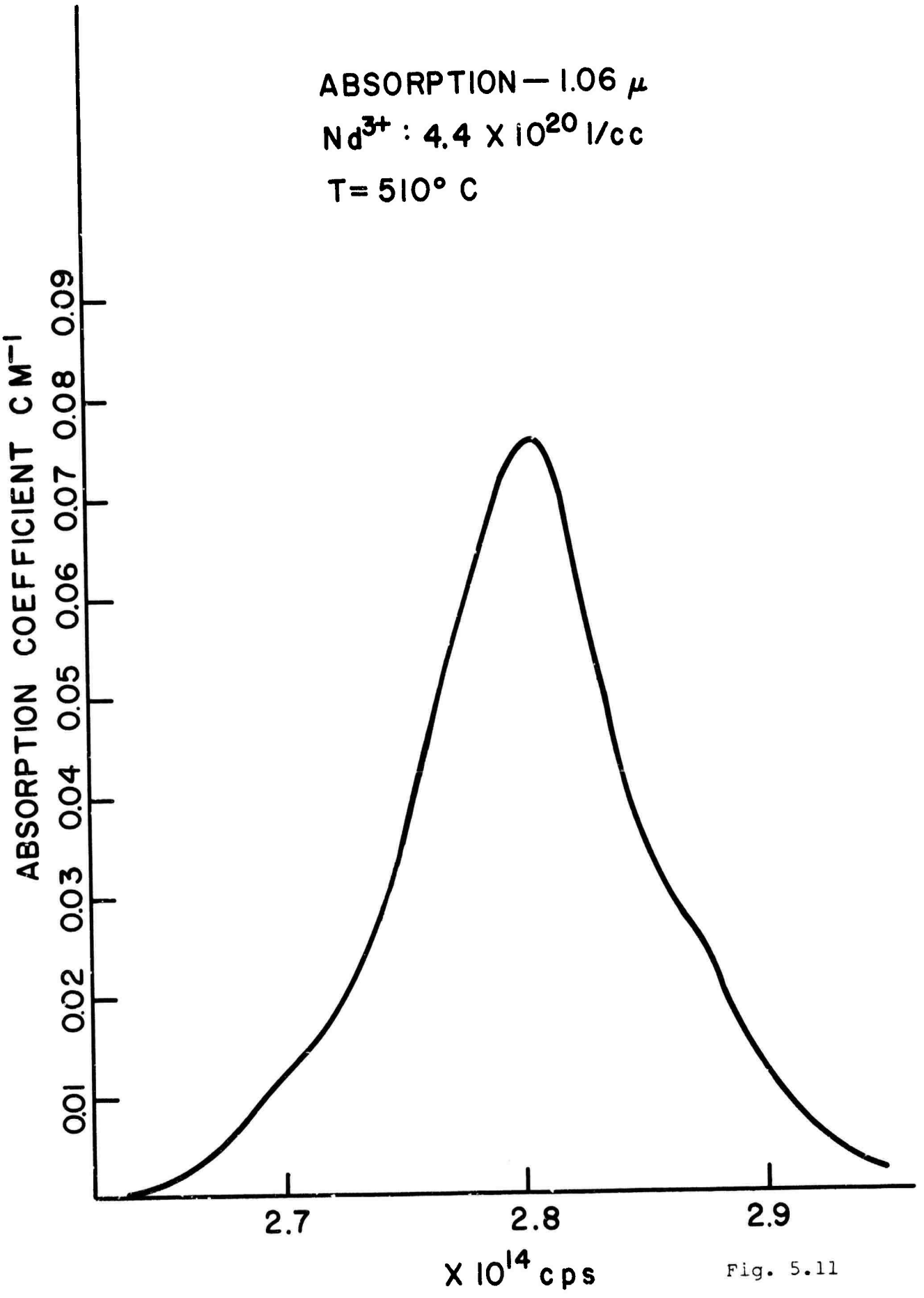
ABSORPTION — 1.06 μ
Nd3+ : 4.4 X 10^20 I/cc
T= 510° C
ABSORPTION COEFFICIENT C M^-1
0.01
0.02
0.03
0.04
0.05
0.06
0.07
0.08
0.09
2.7
2.8
2.9
X 10^14 cps

Fig. 5.11

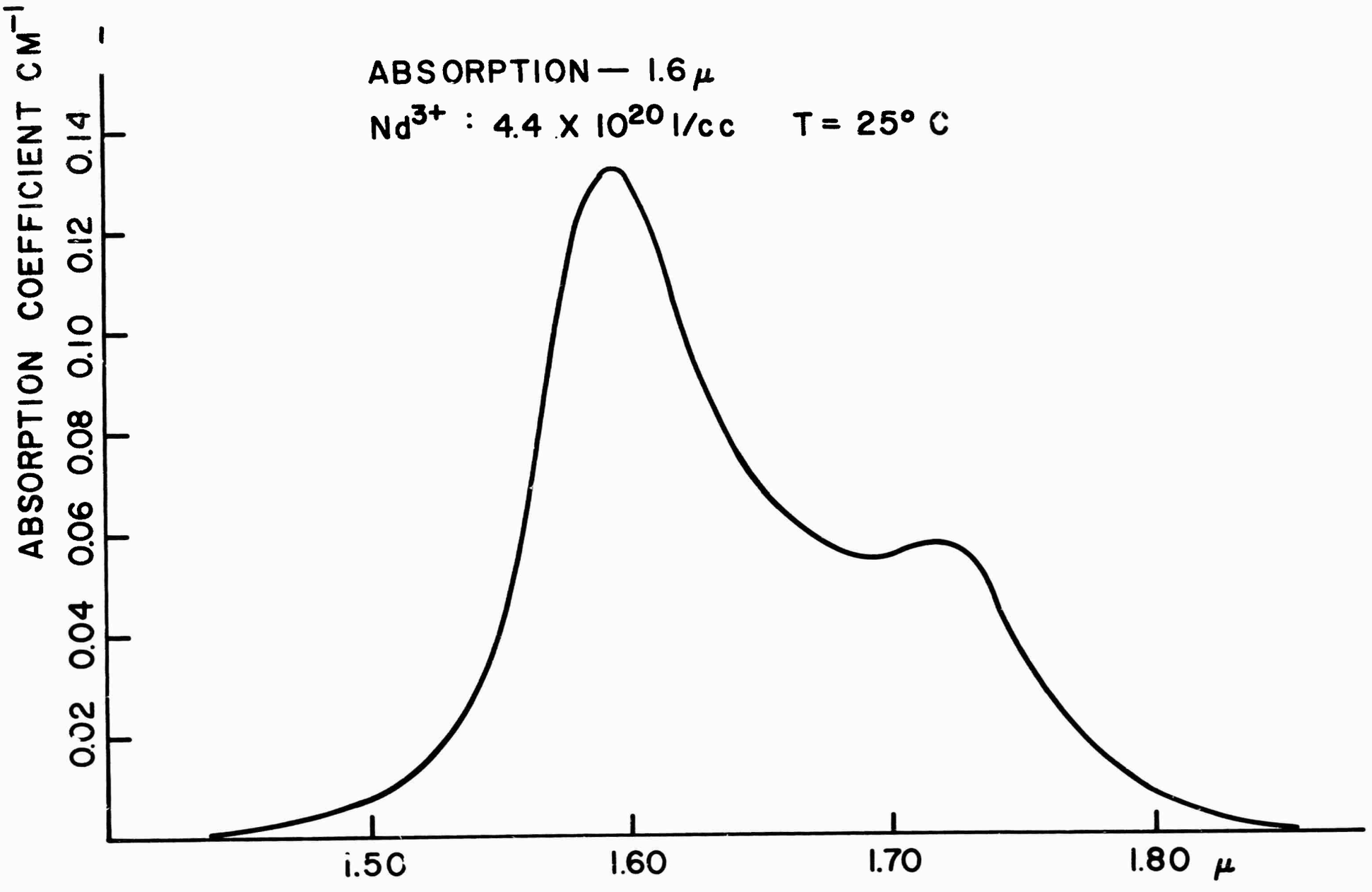
ABSORPTION — 1.6 μ
Nd3+ : 4.4 X 10^20 I/cc T = 25° C
ABSORPTION COEFFICIENT CM-1
0.02 0.04 0.06 0.08 0.10 0.12 0.14
1.50
1.60
1.70
1.80 μ

Fig. 5.12

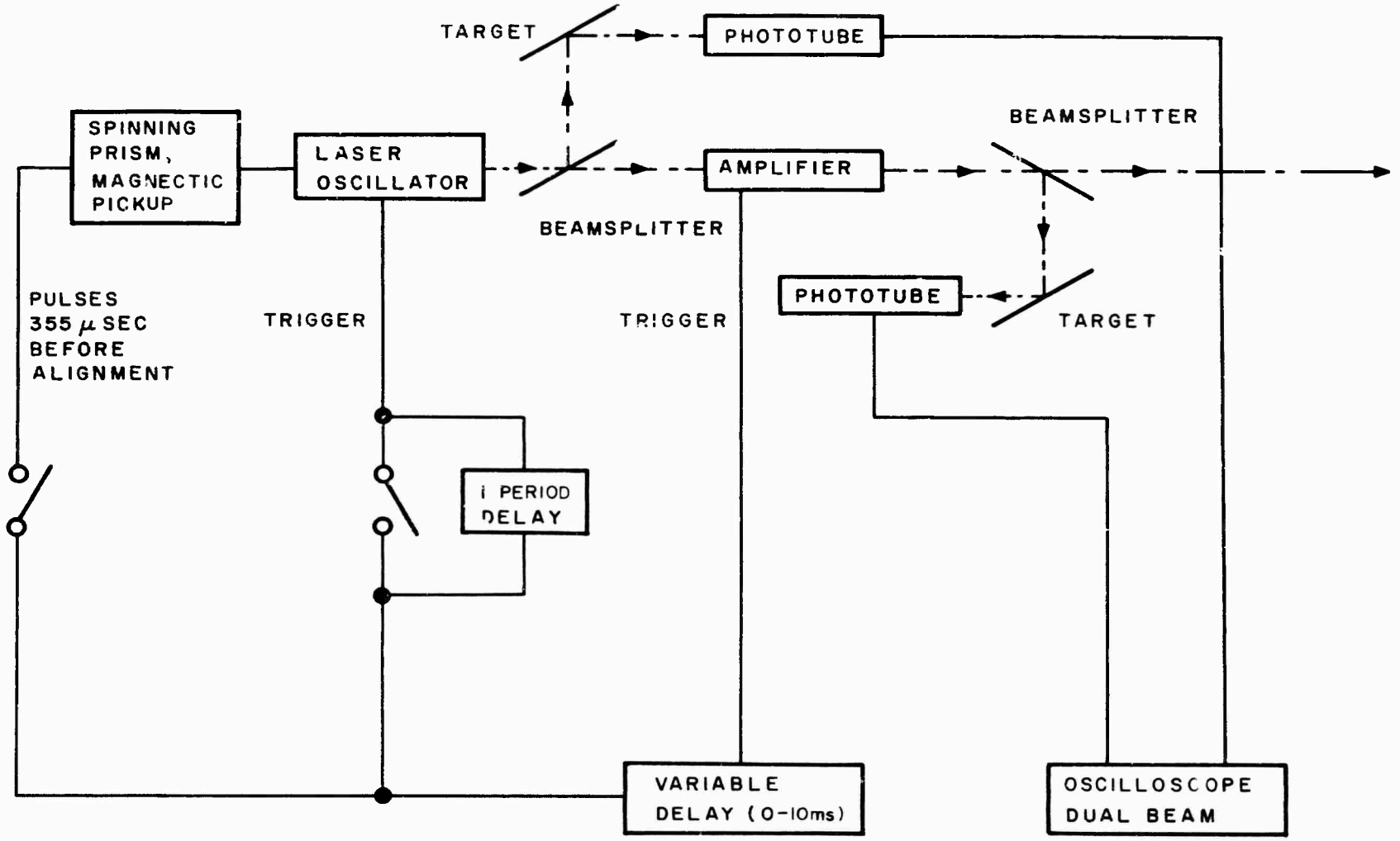

FUNCTIONAL BLOCK DIAGRAM - GAIN MEASUREMENT

Fig. 7.1

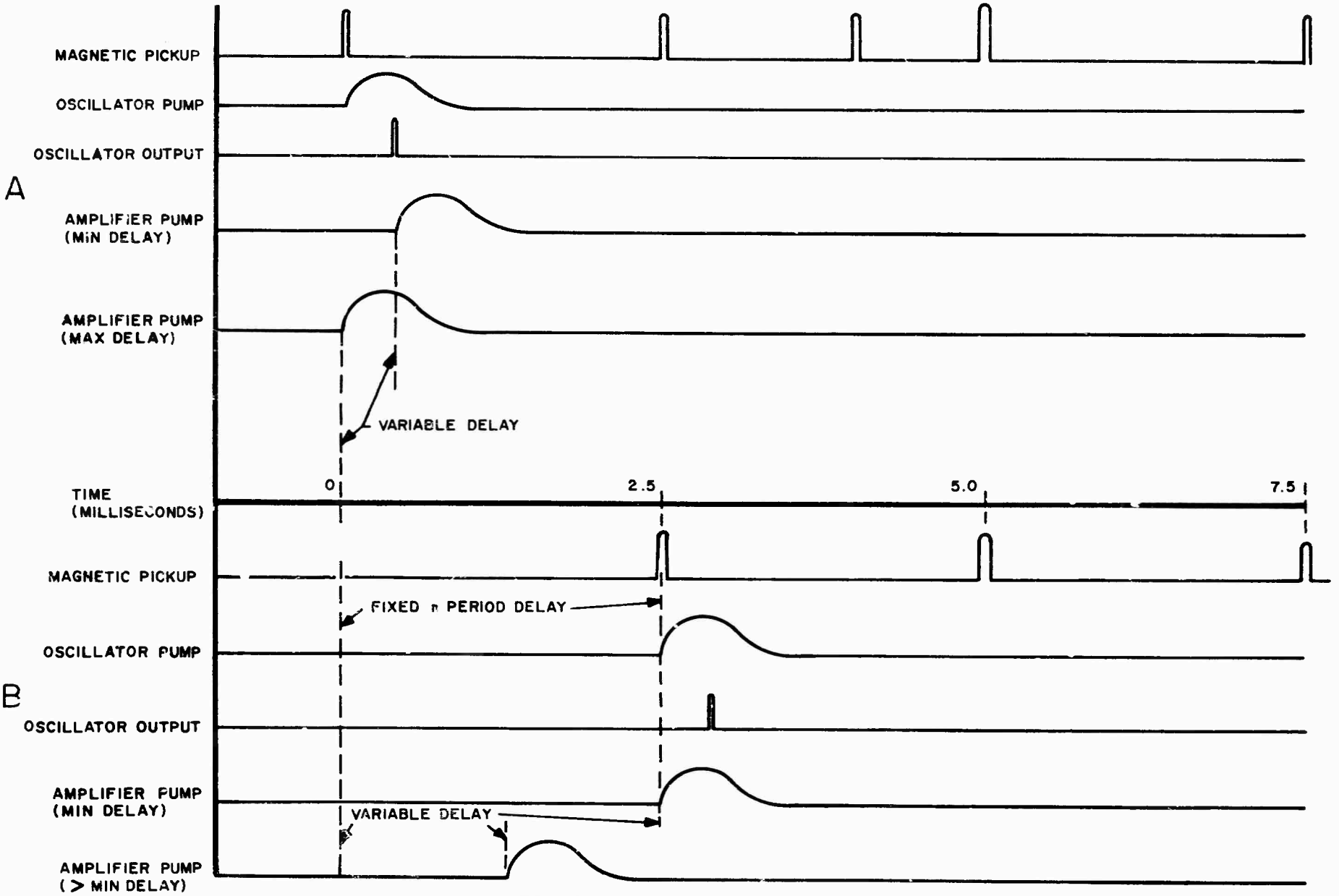

TIMING DIAGRAM OF GAIN MEASUREMENT
A. EARLY PROBING B. LATE PROBING

Fig. 7.2

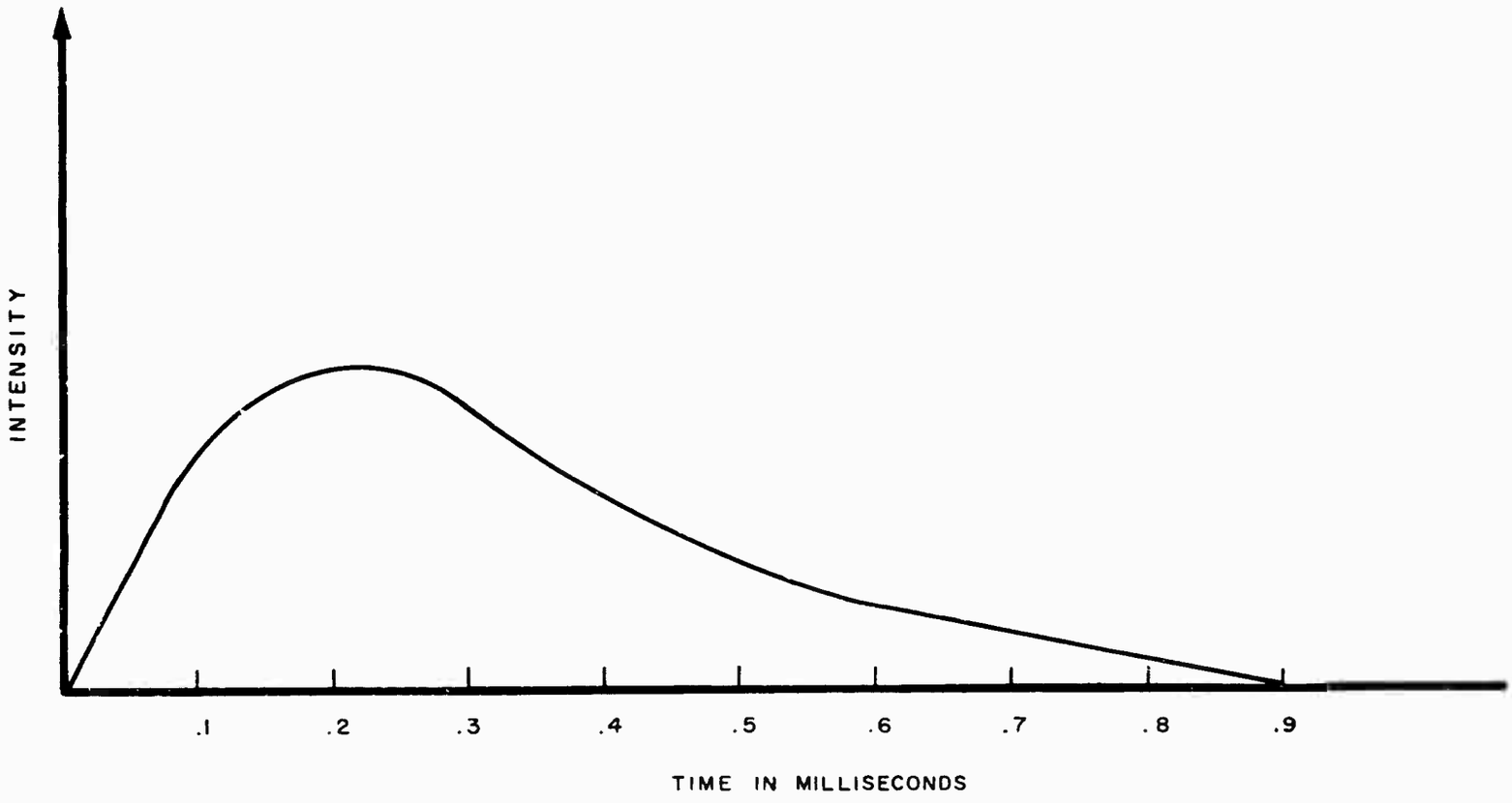

PUMPING WAVEFORM IN AMPLIFIER

Fig. 7.3

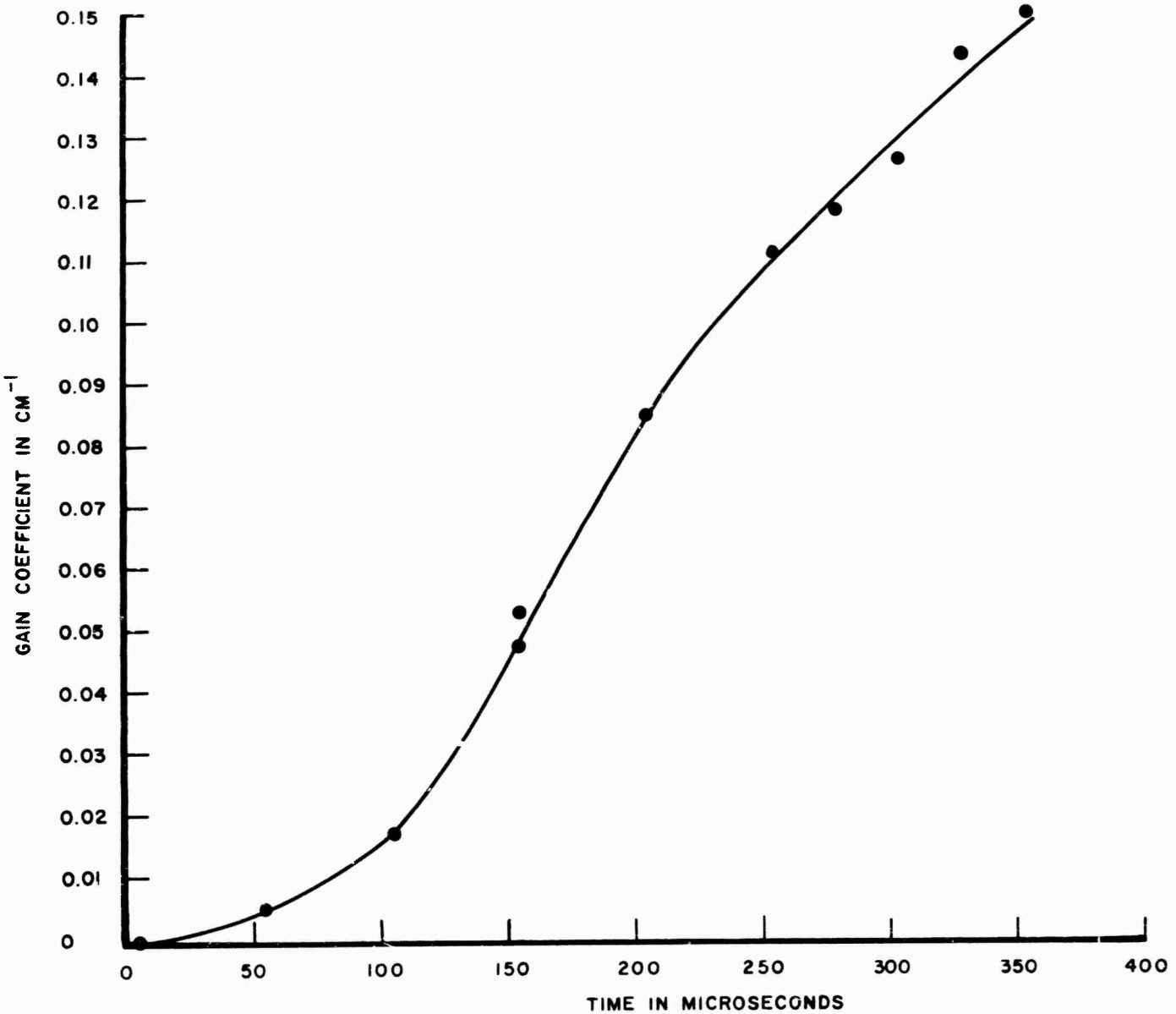

GAIN COEFFICIENT VS. TIME (900 JOULE INPUT)

Fig. 7.4

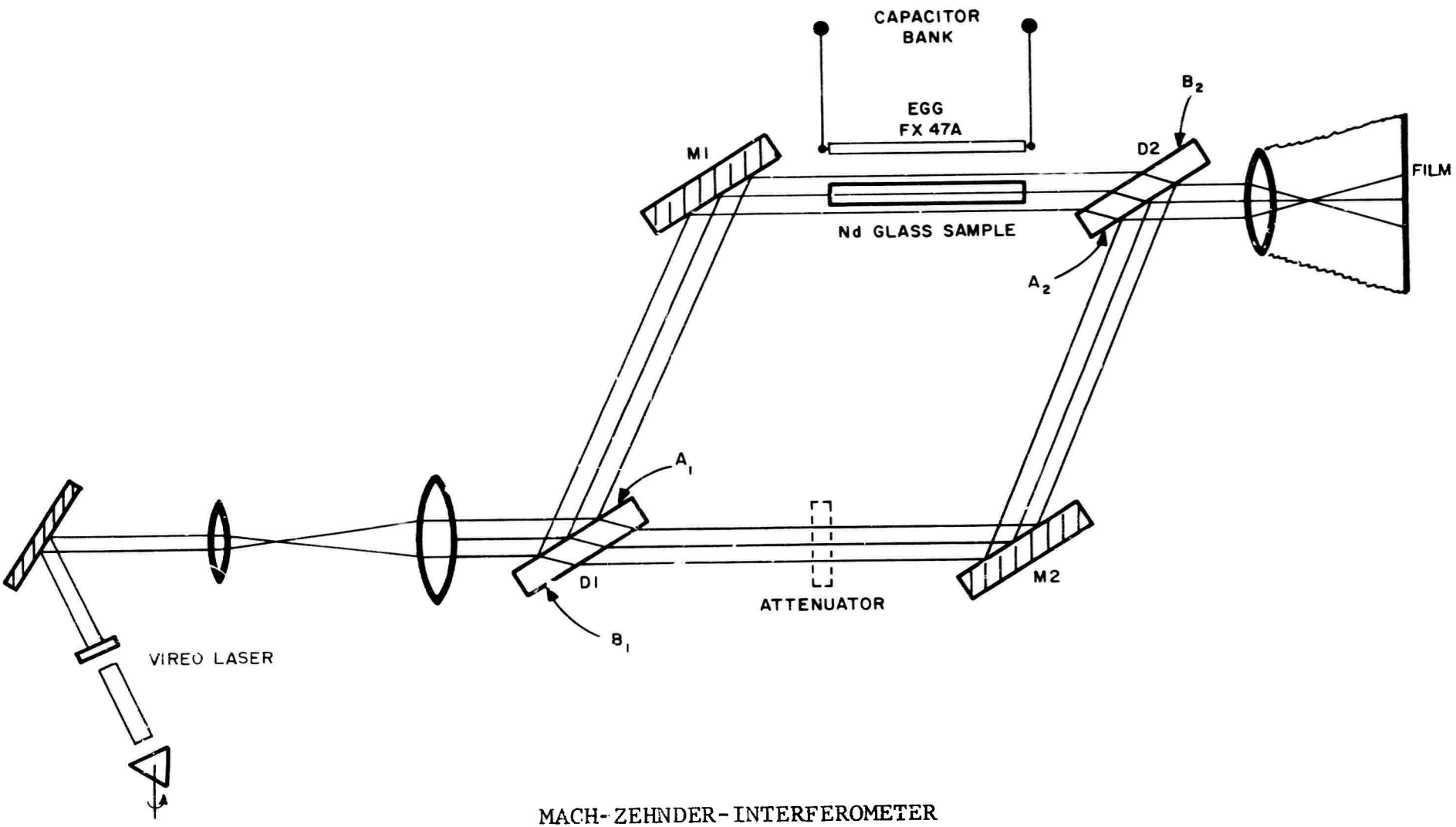

MACH-ZEHNDER-INTERFEROMETER

Fig. 8.1

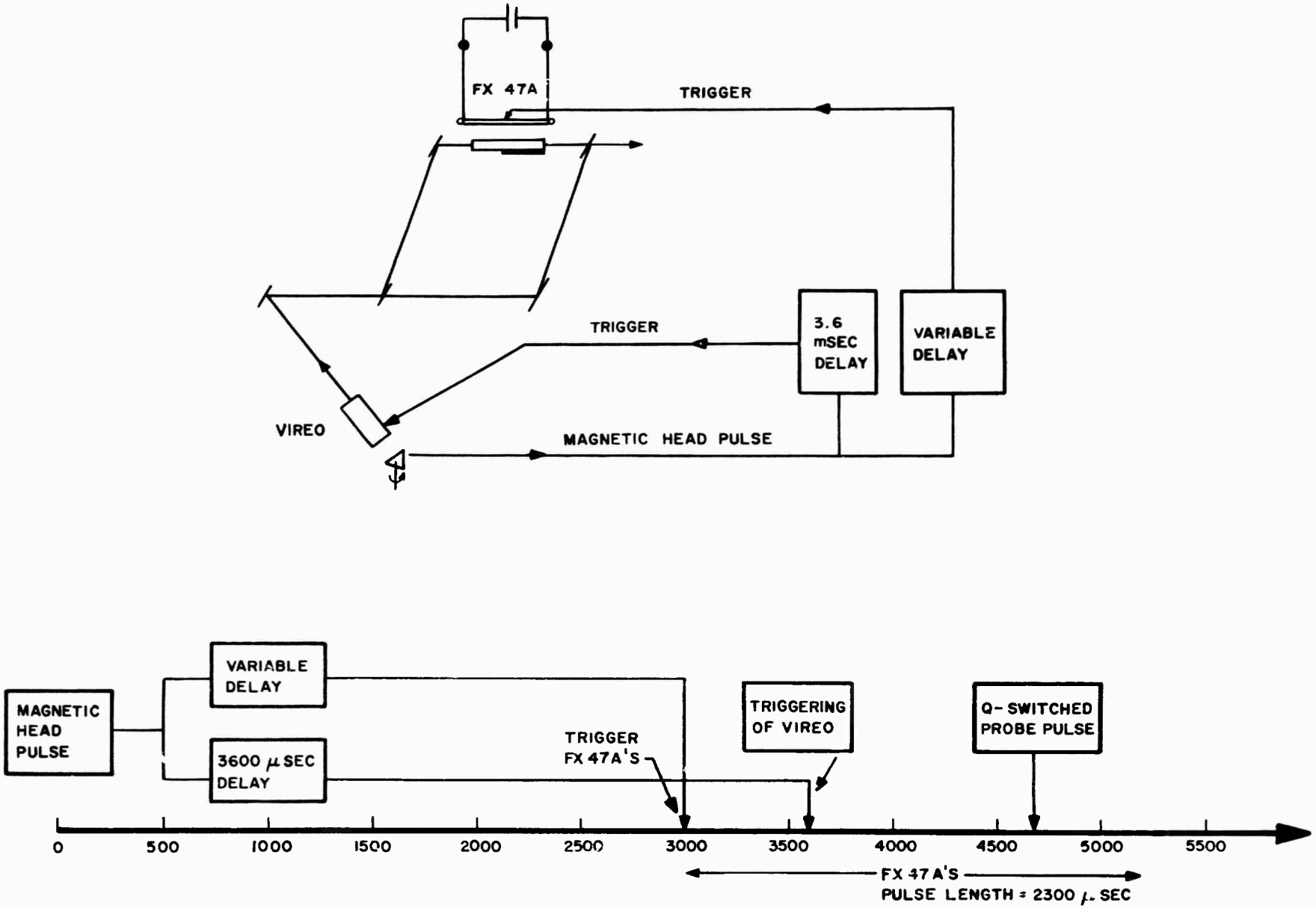

TIMING DIAGRAM

Fig. 8.2

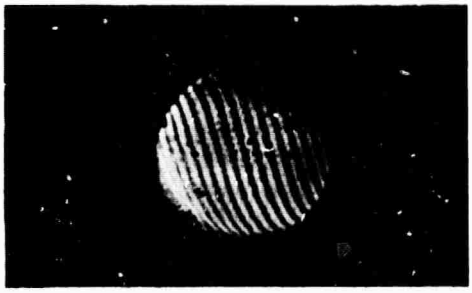

a. Air (No rod in M-Z)

b. t = 0 (Rod in)

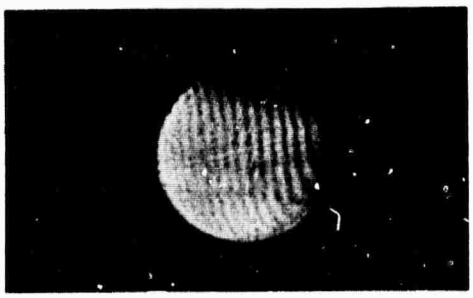

c. t = 200 μsec

d. t = 700 μsec

e. t = 1200 μsec

f. t = 1700 μsec

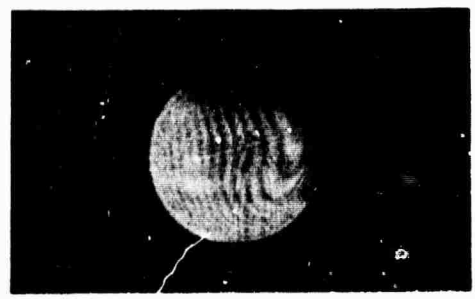

g. t = 2200 μsec

h. t = 2,700 μsec

FIGURE 8.3 GLASS LASER ROD INTERFEROGRAMS AT DIFFERENT TIMES

Note: t = 0 corresponds to start of pump pulse

61-964

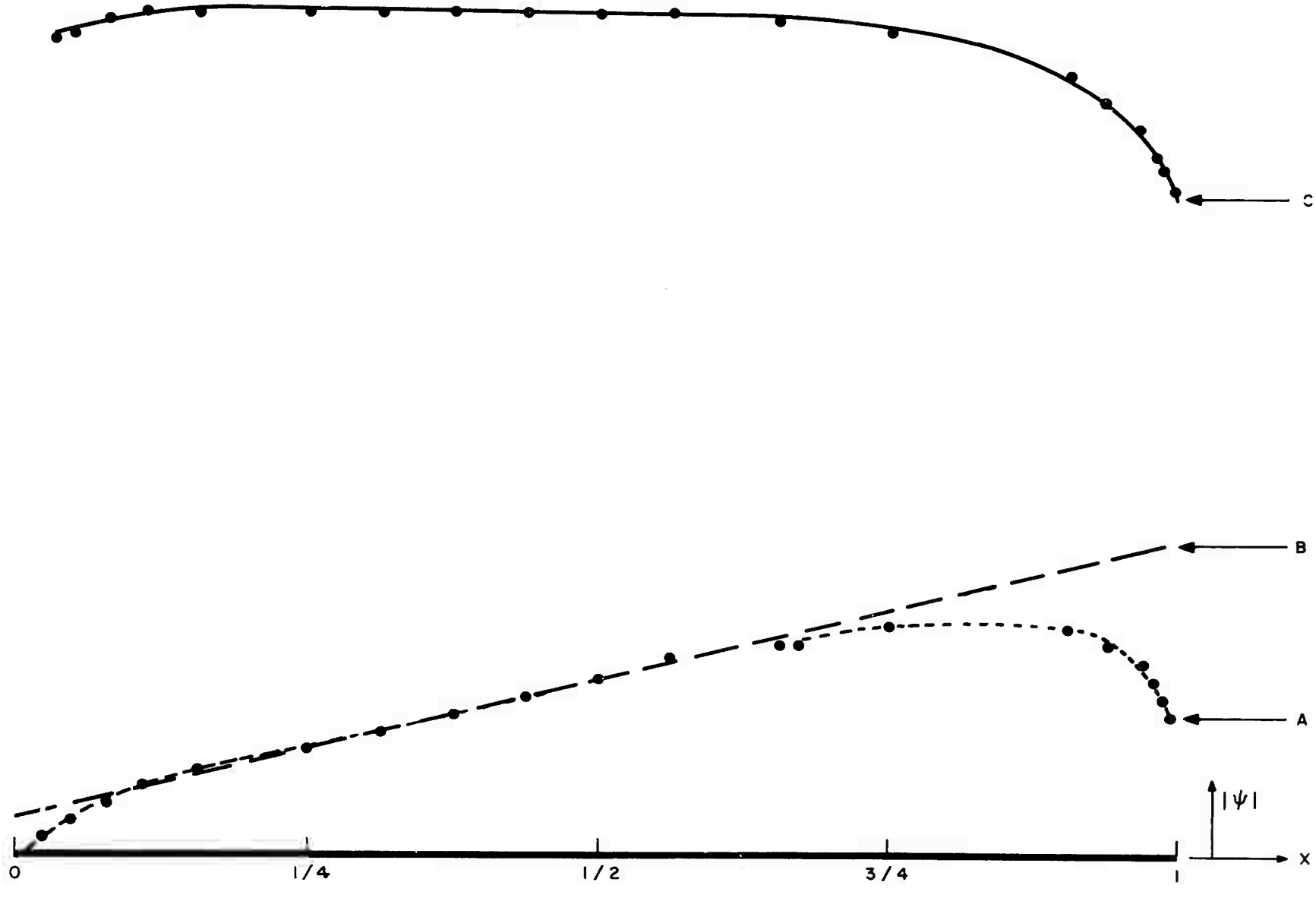

MAPPING OF FRINGE PATTERN PHASE ACROSS APERTURE

Fig. 8.4